



Published in final edited form as:

Cell. 2018 April 19; 173(3): 762–775.e16. doi:10.1016/j.cell.2018.03.076.

GPR68 senses flow and is essential for vascular physiology

Jie Xu¹, Jayanti Mathur¹, Emilie Vessi res², Scott Hammack¹, Keiko Nonomura^{3,†}, Julie Favre², Linda Grimaud², Matt Petrus¹, Allain Francisco³, Jingyuan Li¹, Van Lee¹, Fu-li Xiang¹, James K. Mainquist¹, Stuart M. Cahalan^{3,†}, Anthony P. Orth¹, John R. Walker¹, Shang Ma³, Viktor Lukacs³, Laura Bordone¹, Michael Bandell¹, Bryan Laffitte¹, Yan Xu⁴, Shu Chien⁵, Daniel Henrion², and Ardem Patapoutian^{3,*}

¹Genomics Institute of the Novartis Research Foundation, San Diego, CA 92121, USA

²MITOVASC institute, CARFI facility, CNRS UMR 6015; INSERM U1083; Angers University, Angers, France

³Doris Neuroscience Center, Howard Hughes Medical Institute, The Scripps Research Institute, La Jolla, CA 92037, USA

⁴Department of Obstetrics and Gynecology, Indiana University School of Medicine, Indianapolis, IN 46202, USA

⁵Departments of Bioengineering and Medicine, and Institute of Engineering In Medicine, University of California San Diego, La Jolla, CA 92093, USA

SUMMARY

Mechanotransduction plays a crucial role in vascular biology. One example of this is local regulation of vascular resistance via flow-mediated vasodilation (FMD). Impairment of this process is a hallmark of endothelial dysfunction, and a precursor to a wide array of vascular diseases such as hypertension and atherosclerosis. And yet, the molecules responsible for sensing flow (shear stress) within endothelial cells remain largely unknown. We designed a 384-well screening system that applies shear stress on cultured cells. We identified a mechanosensitive cell line that exhibits shear stress-activated calcium transients, screened a focused RNAi library, and identified GPR68 as necessary and sufficient for shear stress responses. GPR68 is expressed in endothelial cells of small diameter (resistance) arteries. Importantly, Gpr68-deficient mice display

*Correspondence: ardem@scripps.edu.

†Current Address: National Institute for Basic Biology, Division of embryology, 5-1 Higashiyama, Myodaiji, Okazaki, Aichi, 444-8787, Japan

‡Current Address: Vertex Pharmaceuticals Inc., 11010 Torreyana Rd, San Diego, CA 92121, USA

Publisher's Disclaimer: This is a PDF file of an unedited manuscript that has been accepted for publication. As a service to our customers we are providing this early version of the manuscript. The manuscript will undergo copyediting, typesetting, and review of the resulting proof before it is published in its final citable form. Please note that during the production process errors may be discovered which could affect the content, and all legal disclaimers that apply to the journal pertain.

AUTHOR CONTRIBUTIONS

J.X. and A.P. initiated the project and designed experiments. J.X., S.H. and J.K.M. designed and constructed the shear stress stimulation systems. J.X. performed the experiments with the assistance of J.M., K.N., V.L., F.X., S.M., M.B. and S.M.C. E.V. and J.F. performed vessel cannulation experiments. J.L. performed echocardiogram analysis. A.P.O. conducted bioinformatics analysis and picked siRNA library with 2+TM genes. J.R.W. performed RNAseq analysis. J.X., M.B., D.H. and A.P. analyzed the data. J.X. and A.P. wrote the manuscript. A.P. supervised the project.

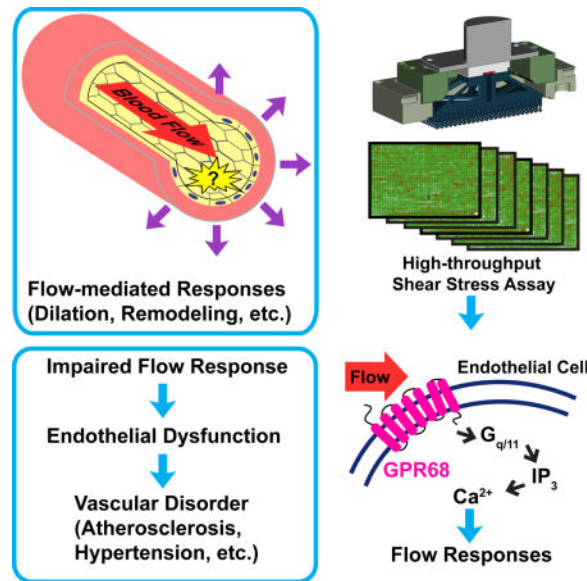
DECLARATION OF INTERESTS

The authors declare no competing interests.

markedly impaired acute FMD and chronic flow-mediated outward remodeling in mesenteric arterioles. Therefore, GPR68 is an essential flow sensor in arteriolar endothelium, and is a critical signaling component in cardiovascular pathophysiology.

In brief

A GPCR is critical for shear stress sensing in blood vessels



INTRODUCTION

Mechanotransduction is the central feature of many biological processes, including the sensing of touch and pain, hearing, cardiovascular dynamics and turgor pressure sensing in bacteria. Several membrane proteins capable of sensing acute mechanical forces have been identified, including the ion channels MscL and MscS in bacteria, the DEGenerin/Epithelial Na⁺ Channel (DEG/ENaC) MEC-4, MEC-10 and Transient Receptor Potential (TRP) channel TRP-4 in *C. elegans*, and NOMPC in *Drosophila* (Driscoll and Chalfie, 1991; Huang and Chalfie, 1994; Kang et al., 2010; Levina et al., 1999; Li et al., 2006; Sukharev et al., 1994; Walker et al., 2000; Yan et al., 2013).

In vertebrates, the identity of mechanosensors has been more elusive. First identified in mammals, Piezos are a family of mechanically-activated ion channels conserved through evolution (Coste et al., 2010). Piezos play crucial roles in various physiological settings, e.g., vascular development and function, and somatosensation (Li et al., 2014; Lukacs et al., 2015; Nonomura et al., 2017; Ranade et al., 2014; Retailleau et al., 2015; Wang et al., 2016; Woo et al., 2014). Within the vascular system, Piezo1 in smooth muscle cells plays a role in hypertension-dependent arterial remodeling (Retailleau et al., 2015). In endothelial cells, Piezo1-deficiency causes compromised flow-mediated vasodilation and increased systolic blood pressure (Wang et al. 2016). However, another report did not find evidence for hypertension in Piezo1-deficient mice, and show a requirement of Piezo1 in flow-mediated

vasoconstriction instead (Retailleau et al., 2015; Rode et al., 2017; Wang et al., 2016). Regardless of the precise role of Piezo1, an understanding of how blood vessels sense shear stress or pressure is in its infancy.

Beyond ion channels, G protein-coupled receptors (GPCRs) are sensory molecules responsible for vision, smell, and taste, among other functions. In addition, a number of GPCRs, including Angiotensin II receptor type 1 (AGTR1), bradykinin receptor B2 (BDKRB2) and parathyroid hormone 1 receptor (PTH1R), have been proposed as mechanosensors in various physiological settings, including cardiovascular physiology. (Chachisvilis et al., 2006; Mederos y Schnitzler et al., 2008; Zhang et al., 2009). However, evidence that these GPCRs are both necessary and sufficient for acute mechanotransduction in an *in vivo* setting is lacking. Regardless, there is evidence that GPCR signaling is important for mechanotransduction in vasculature physiology. For example, acute shear stress imposed by blood flow on vessel endothelial cells induces diverse downstream signaling events, most notably the phospholipase C (PLC)-dependent increase in intracellular calcium concentrations mainly via unknown mechanisms (Ishida et al., 1997; Melchior and Frangos, 2012). However, the identity of the putative mechanosensitive GPCRs *in vivo* remains unknown.

Finally, beyond hearing, somatosensation, and vascular biology, many other cell types within bone, muscle, lung, kidney, eye, and other tissues respond to mechanical stimuli through unknown mechanisms (Jalouk and Lammerding, 2009). We previously conducted a functional genomic small interfering RNA (siRNA) screen to identify Piezo1 using membrane indentation and electrophysiological recording (Coste et al., 2010). It was a low-throughput screen that required a year to identify Piezo1 after screening 71 other candidate genes. Here we aimed to accelerate genomic screens relevant to mechanotransduction by designing a novel high-throughput (HT) mechanical stimulation system. Using this novel assay, we identified a *bona fide* shear stress sensor GPR68, and show that it plays a crucial role in vascular physiology and pathophysiology. These findings demonstrate that GPCRs as well as ion channels can function as *in vivo* shear stress sensors.

RESULTS

A novel 384-well mechanical stimulation assay

We aimed to accelerate genomic screens relevant to mechanotransduction by designing a novel high-throughput (HT) mechanical stimulation system. Among different types of mechanical forces, fluid shear stress is perhaps the most amenable to a HT assay format, and physiologically relevant flow sensors in vascular biology are mainly unknown. Our design concept featured a flat-headed piston driven by an acoustic transducer controlled by a signal generator (Figure 1A). During operation, the piston was immersed in buffer in a transparent-bottom well plate, moving up and down at commanded frequency and amplitude to create disturbed fluid motion with an oscillatory fashion. The moving fluid imposes shear stress on the cells cultured at the bottom of the chamber. The response of the cells can be imaged by a detector below the plate (Figure 1A). After validation, we scaled up the system to 384-well format by 3D printing a 384-pin stimulation array and then affixed to an acoustic transducer (Figure 1B). We optimized the shape of the pins to avoid trapping air bubbles in the plate

(Figure 1B, right). The system fit inside the Molecular Devices Fluorescent Image Plate Reader (FLIPR Tetra) (Figure 1C, D). We measured the intensity of the shear stress generated by the HT system using particle image velocimetry and found that it is between 0.1~2 Pa (Ranade et al., 2014). We can increase the intensity of the shear stress up to ~16.7 Pa by increasing the viscosity of the buffer using polyvinylpyrrolidone (PVP), a bio-compatible, water-soluble polymer.

Next, we asked if Human Umbilical Vein Endothelial Cells (HUVECs) could be acutely activated by the HT system using intracellular calcium levels as a readout. HUVECs express endogenous PIEZO1 and show PIEZO1-dependent alignment to the direction of flow (Li et al., 2014; Ranade et al., 2014). Indeed, we observed robust transient increase in intracellular calcium levels in HUVECs when stimulated with shear stress at 6.5 Pa and above (with increased viscosity by PVP) (Figure 1E). The shear stress-induced calcium transients were completely abolished by 2.5 mM EGTA, suggesting that the signal was caused by extracellular calcium entering the cells (Figure 1E). The response was greatly attenuated in cells treated with PIEZO1 siRNA (Figure 1F, G). These results demonstrate that our HT mechanical stimulation system is capable of applying physiologically relevant shear stress in a precise, quantitative, and reproducible fashion.

MDA-MB-231 breast cancer cells express an unknown shear stress sensor

We set three criteria for a cell line suitable for the high-throughput siRNA screen of novel mechanosensitive receptors: a) must respond to our HT flow system by displaying calcium transients, b) must be transfectable by siRNA with satisfactory knockdown efficiency, and c) the response to shear stress should not depend on PIEZO1 or PIEZO2. We compiled a list of candidate cell lines based on the National Cancer Institute 60 human tumor cell line collection (NCI-60). We selected cell lines that have low levels of RNA transcripts of PIEZO1 and PIEZO2 with the data from [BioGPS.org](https://biogps.org). Out of the 25 cell lines tested, the lung cancer cell line A549 and the breast cancer cell line MDA-MB-231 showed shear stress-evoked calcium transients (Figure 2A). MDA-MB-231 responded to disturbed shear stress of 2 Pa with robust signals, while those of A549 were relatively modest (Figure 2A). The signal in MDA-MB-231 cells was mostly abolished when the calcium stores of the cells were depleted by thapsigargin. Removing extracellular Ca^{2+} by incubating the cells with EGTA prior to the onset of shear stress greatly reduced but did not abolish the response (Figure 2B, C). This suggests that the calcium transients are store-dependent and also partly depends on the entry of calcium from the intracellular space. Transfecting MDA-MB-231 cells with siRNA against PIEZO1 or PIEZO2 achieved 86% and 78% knockdown at the transcript level, respectively, and did not affect the shear stress response of MDA-MB-231 cells, suggesting an unknown molecule is responsible for sensing shear stress (Figure 2D).

GPR68 is required for shear stress responses in MDA-MB-231 cells

We focused on membrane-integrated proteins as the most probable candidates for novel mechanosensors. We constructed a library of siRNAs against genes encoding proteins with two or more predicted transmembrane domains (2+TM), a characteristic trait shared by ion channels and GPCRs. The library contains 21,925 unique siRNAs, targeting 3,175 unique reference sequences encoded by 2,765 unique genes, arranged in a singlet configuration, *i.e.*,

each well of the 384-well plate contains one siRNA oligo. On average, each gene is represented by 8 siRNAs across the library, most of them located on different plates. We transfected the MDA-MB-231 cells with the siRNA library and carried out the screen using the HT shear stress system. The primary screen yielded 56 hits, of which 26 were reconfirmed in a secondary screen. Of the 26 genes, GPR68 was the only one in the final confirmation run to show significantly reduced calcium transients caused by disturbed shear stress upon knockdown (Figure 3A). siRNAs targeting different regions of GPR68 were all effective in inhibiting the signal, suggesting that attenuation is not likely due to off-target effects (Figure 3B).

GPR68 was described to be a proton-activated GPCR. It is fully activated at pH 6.8 and is mostly inactive at pH 7.8 (Ludwig et al., 2003). Indeed, MDA-MB-231 cells showed little intracellular calcium increase to pH 7.4 and above, while the response was maximal to stimulation by pH 6.5 and below (Figure 3C). Knocking down GPR68 significantly reduced proton-induced response (Figure 3D). We next tested shear stress response of MDA-MB-231 cells at various pH levels. We observed a bell-shaped curve such that shear stress is most effective at pH levels of 7.4-6.9 (normal arterial blood pH is ~7.4, and 6.9 represents severe acidosis) (Figure 3E) (Schwaderer and Schwartz, 2004). This suggests that GPR68 requires the presence of protons to sense shear stress. It was suggested that protonation leads to loss of bonding and repulsion between extracellular histidines, allowing the receptor to adopt an active conformation at physiological pH (Ludwig et al., 2003). We therefore tested a mutant of GPR68 where histidine 17, 20, 84, 169 and 269 were changed to phenylalanine, and found that it lost both pH sensitivity and shear stress sensitivity (Figure S2A), supporting the notion that appropriate levels of proton must be present for the receptor to be activated. Hence, all follow-up experiments were carried out at pH 7.4.

GPR68 is activated by shear stress imposed by disturbed and laminar flow

To test if GPR68 activation is sufficient to confer mechanosensitivity, we transiently transfected GPR68 in HEK-293T cells and applied shear stress. HEK cells expressing human GPR68 showed an increase in intracellular calcium levels in response to 2 Pa shear stress, while vector-transfected cells were not responsive (Figure 4A). The amplitude of the calcium signals was dependent on the intensity of shear stress applied (Figure 4B). The maximum amplitude of the shear stress response is ~70% of the response when stimulated with extracellular proton at pH 6.5 (Figure 4C), implying that shear stress responses are overall comparable to the acid responses. The slightly lower response may be due to the fact that not all GPR68 proteins on the cell membrane experience shear stress as they would experience changes in pH. Notably, the responses were completely abolished by U73122, a PLC inhibitor, suggesting that the signal is indeed dependent on the activity of GPR68, a $G_{q/11}$ -coupled receptor (Figure 4D). Proton-induced GPR68 activity is acutely blocked by Cu^{2+} (Ludwig et al., 2003), and 20 μM Cu^{2+} also blocked the shear stress-induced calcium signal (Figure 4D). This acute blockage of shear stress response argues against the possibility that overexpression of GPR68 causes alterations in HEK cells that indirectly induce mechanosensitivity. One possible mechanism is that shear stress causes a decrease in pH, which in turn activates GPR68 indirectly. We measured both extracellular and intracellular pH real time by fluorescence imaging and found no change in either upon the

application of shear stress (Figure S2B–D). Together, our data provide evidence for a necessary and sufficient role of GPR68 in the shear stress-induced release of calcium from stores.

Many GPCRs have been proposed to be mechanosensitive, although direct activation by mechanical forces (on the order of seconds) has not been demonstrated using intracellular calcium as a readout (Storch et al., 2012). To test if sensitivity to shear stress of GPR68 is unique among GPCRs, we selected human GPCR clones that are considered mechanosensitive, including angiotensin II receptor type 1 (AGTR1), arginine vasopressin receptor 1A (AVPR1A), bradykinin receptor B2 (BDKRB2), muscarinic cholinergic receptor 5 (CHRM5), endothelin receptor type A (EDNRA), histamine receptor H1 (HRH1) and parathyroid hormone 1 receptor (PTH1R). These are $G_{q/11}$ -coupled receptors that cause an increase in the intracellular calcium levels through the mobilization of calcium from intracellular stores upon activation. We transfected HEK-293T cells with these GPCRs and subjected them to disturbed shear stress at 2 Pa. No significant increase in intracellular calcium levels was detected in cells transfected with GPCRs other than human GPR68. We demonstrated functional expression of these receptors by evaluating their response to known agonists (Figure 4F). Finally, we tested GPR132, the closest family member of GPR68, and also a $G_{q/11}$ -coupled receptor, and found that it is not responsive to the same level of shear stress, while it did respond normally to its agonist lactate (Figure 4E, F)(Chen et al., 2017). These results highlight the unique sensitivity of GPR68 to disturbed shear stress.

Fluid flow *in vivo* can be laminar or disturbed. In laminar flow, the fluid flows in parallel layers in an orderly fashion (Chiu and Chien, 2011) and can be pulsatile or steady. In contrast, disturbed flow has irregular fluctuations with time and no clear direction. We tested if GPR68 responds to shear stress imposed by pulsatile laminar flow. With 1 Hz pulsatile laminar flow at 3.4 Pa, Gpr68-transfected HEK-293T cells showed a robust increase of intracellular calcium levels. In most cells, the calcium level returned to baseline within minutes after the flow stopped. Non-transfected cells in the same chamber did not respond (Figure 4G, H). There were large, periodic fluctuations in calcium signals in both Gpr68-transfected cells and untransfected cells synchronous with the flow pulsatility. These are artifacts caused by the cyclic shift in optical focus as a result of the expansion and contraction of the plastic flow chamber in response to the pulsatile flow. We also assayed the cells' response to steady laminar flow. Robust responses were also observed with steady laminar flow in the transfected cells, but not in the non-transfected cells (Figure 4I, J).

Several proteins that are implicated as sensors of laminar flow, including TRPV4, PIEZO1, AGTR1 and BDKRB2 (Chachisvilis et al., 2006; Li et al., 2014; Mendoza et al., 2010; Ramkhalawon et al., 2013). None of those caused any significant increase in calcium levels with the same flow stimulation when expressed in HEK cells (Figure 4K).

GPR68 is expressed in endothelial cells of small-diameter arteries

GPR68 is evolutionally conserved among vertebrates. No orthologues are found in bacteria, fungi, plants or invertebrates. In mouse, Gpr68 mRNA is detected in a variety of tissues (Figure 5A). The expression level is highest in the spleen, consistent with previous reports that Gpr68 transcripts are enriched in immune cells (Yan et al., 2014). We tested a number of

commercially available antibodies against Gpr68 and found that none of them can specifically detect the heterologously-expressed Gpr68. Therefore we employed *in situ* hybridization to detect Gpr68 transcripts in tissue sections. Interestingly, we found that Gpr68 mRNA is detected in small diameter blood vessels across a number of tissues, including pancreas, liver and brain (Figure 5B). Based on morphology, the Gpr68+ cells appear to be endothelial cells. To determine the identity of those cells, we obtained an eGFP reporter line of Gpr68 generated by the GenSat Project (Figure 5C). We first tested if the eGFP reporter faithfully represents endogenous Gpr68 expression. We isolated immune cells from the spleen of the reporter mice and C57 B/L6 mice, and subjected them to fluorescence-activated cell sorting (FACS). GFP signal was detected in most CD8+ T cells, NK cells and a subset of CD4+ cells. No GFP signal was detected in B cells (Figure S3A). qRT-PCR of the RNA isolated from sorted cells of C57 B/L6 mice showed that Gpr68 transcript levels are high in CD8+ T cells and NK cells, intermediate in CD4+ cells, and absent in B cells (Figure S3B). These results indicate that the GFP signal accurately represents endogenous Gpr68 transcription. Next, we tested if GFP signal is detected in endothelial cells. We isolated primary vascular endothelial cells from the mouse bladder and sorted cells that are positive for CD31 (endothelial cells) and negative for CD45 (leukocytes). We observed both GFP+ and GFP- populations of endothelial cells (Figure 5D, green and grey population, respectively). RNASeq with GFP+ and GFP- endothelial cells showed that Gpr68 transcripts are enriched nearly 8 fold in GFP+ cells. In comparison, Piezo1 is expressed at similar levels across the two populations. These results validate that GFP levels accurately represent endogenous Gpr68 expression in endothelial cells.

We next evaluated Gpr68 expression pattern by staining a panel of tissue sections from eGFP reporter mice using a GFP antibody. The antibody stains endothelial cells in pancreas, liver and bladder, among other tissues (Figure S3C, D, E). Consistent with the FACS result, we detected GFP only in a subset of endothelial cells (Figure S3D, E). Interestingly, the GFP+ cells appear to be endothelial cells of arterioles, the small diameter arteries surrounded by a layer of relatively thick smooth muscles. The venules, which have a less prominent smooth muscle layer, are mostly negative for GFP staining (Figure S3D, E). This is further confirmed by staining sections of mesenteric vessels. The GFP signal was not detected in 1st and 2nd order arteries. The endothelial cells of 3rd order arterioles and the arterioles in the wall of small intestine showed the strongest GFP antibody staining (Figure 5F). These results indicate that Gpr68 is preferentially expressed in small-diameter resistance arteries, the major sites of regulation of resistance to blood flow, suggesting that Gpr68 may play a role in flow-mediated vasodilation.

GPR68 is required for laminar shear stress responses of mouse primary microvascular endothelial cells

The striking expression pattern of Gpr68 predicts that the GFP+ endothelial cells should respond to shear stress. To test this, isolated mouse primary microvascular endothelial cells (MVECs) from the cerebrum of homozygous Gpr68-eGFP reporter mice and assayed their response to shear stress in the flow chamber. 1 Hz pulsatile laminar flow was applied with increasing intensity of 2 Pa, 4 Pa and 6 Pa (physiologically relevant levels of shear stress experienced by small arteries). GFP+ endothelial cells responded to the flow by increasing

intracellular calcium levels, while the GFP⁻ cells showed significantly lower responses (Figure 6A). To test if the flow response is dependent on Gpr68, we carried out knockdown experiments with viruses containing Gpr68 small hairpin RNA (shRNA) and non-targeting shRNA. Upon stimulation with pulsatile flow at 4 Pa, the GFP⁺ cells infected with non-targeting shRNA virus showed an increase in intracellular calcium levels, while cells infected with Gpr68 shRNA virus showed no appreciable responses (Figure 6B). Importantly, GFP⁺ cells infected with either virus showed similar response to 50 μ M ATP, demonstrating that these cells are healthy and able to respond to chemical stimuli (Figure 6C). qRT-PCR demonstrated that the RNA level of Gpr68 was knocked down by 73% in the Gpr68 shRNA-treated endothelial cells, compared to the non-targeting shRNA-treated cells (Figure 6D). These results show that the endogenous Gpr68 in primary MVECs are necessary for flow-induced calcium transients.

Gpr68 is required for flow-mediated dilation responses of mouse small-diameter mesenteric arteries *ex vivo*

The endothelial cells in resistance arteries sense increase in blood flow and signal to smooth muscles via Nitric Oxide (NO), Endothelium-derived hyperpolarizing Factor (EDHF) and other mechanisms to cause their relaxation (Niebauer and Cooke, 1996). This results in an increase in the diameter of the vessel and is called flow-mediated dilation (FMD). To investigate whether GPR68 is responsible for FMD, we isolated mesenteric arteries (MAs) from the Gpr68 KO mice and performed *ex vivo* cannulation experiments. Compared to WT littermates, Gpr68 KO mice had significantly lower FMD response in 3rd order MAs (Figure 7A, but not in 1st and 2nd order MAs (Figure S4A, B). This matches the expression pattern of Gpr68 in the mesenteric vessel bed (Figure 5F). Nitric oxide synthase (NOS) inhibitor L-NAME almost completely abolished FMD response in 3rd order MAs of both KO and WT animals, indicating that Gpr68 likely functions upstream of the NO pathway (Figure S4C). Notably, in 3rd order MAs, dilation to acetylcholine and constriction to KCl were similar between KO and WT mice (Figure S4D), indicating that loss of Gpr68 activity specifically affects the mechanical aspect of the dilation response in 3rd order MAs.

Since loss of Gpr68 activity leads to impaired FMD response in 3rd order MAs, we predicted that activating Gpr68 by chemical means only (*i.e.*, without flow) would lead to vessel dilation. We synthesized an allosteric modulator of GPR68 named Ogerin, which was shown to specifically modulate human and mouse GPR68 activity (Huang et al., 2015). We found that Ogerin activates Gpr68 expressed in HEK-293T cells, with an EC₅₀ around 0.17 μ M (Figure S5). Consistent with our prediction, adding Ogerin to 3rd order WT MAs induced a dose-dependent dilation (Figure 7B). Importantly, similar vessels from KO mice displayed no dilation response to Ogerin across a concentration range from 1 nM to 1 μ M (Figure 7B).

Gpr68 KO mice are grossly normal (Yan et al., 2014). Our echocardiography study showed that they have similar cardiac parameters compared to WT littermates (Figure S6A). We also measured hemodynamic parameters in Gpr68 KO mice and found slightly lower systolic pressure, while diastolic pressure, mean arterial pressure and heart rate were indistinguishable from WT mice (Figure S6B). The marginally lower systolic blood pressure phenotype could be due to compensatory mechanisms, which might cause a lowering of the

baseline vascular tone or an increase in the effectiveness of alternative dilation mechanisms. Indeed, we found that the myogenic tone was lower in 3rd order arteries from Gpr68 KO mice (Figure S6C). In addition, the dilation response to nitric oxide donor sodium nitroprusside (SNP) is higher in KO vessels, suggesting that KO mice could be more sensitive to NO-induced vasodilation (Figure S6D).

GPR68 is required for flow-mediated outward remodeling of mouse small-diameter mesenteric arteries *in vivo*

Chronic increase in flow induces a diameter enlargement in vessels and this flow-mediated outward remodeling (FMR), driven by the rise in shear stress, has a major role in post-ischemic revascularization (Henrion et al., 1997). To test if GPR68 is required for FMR, we performed ligation of second order mesenteric vessels to create a branch of arteries with high flow (HF, Figure 7C). We found that FMR was absent in 3rd order MAs isolated from GPR68 KO mice, compared to WT mice where the increase in flow induced a significant diameter increase (Figure 7D–F). Importantly, FMR in 1st order arteries of GPR68 KO mice was not different from that observed in WT mice (Figure S7A, B, C), suggesting GPR68's shear stress-sensing role is specific to small-diameter arteries (resistance arteries, where GPR68 is expressed).

DISCUSSION

GPR68 is a mechanosensor

To categorize a protein as a mechanosensor, several criteria should ideally be met: expression in the correct cells, essential for the immediate signaling response of cells to the relevant force, and activation by the relevant mechanical force when expressed in heterologous cells or reconstituted in lipid bilayers (Ernstrom and Chalfie, 2002). Here we provide evidence that GPR68, a Class A Rhodopsin-like GPCR, satisfies all three criteria for a mechanosensor. Gpr68 is expressed in a subset of vascular endothelial cells that have a significant response to shear stress. It is required for shear stress-sensitivity of endothelial cells. Finally, overexpressing human or murine Gpr68 in naïve HEK-293T cells induces sensitivity to shear stress in response to physiologically-relevant types of flow stimulations.

Compared to other putative mechanosensitive GPCRs tested, only GPR68 overexpression gives rise to detectable levels of calcium transients in response to disturbed and laminar shear stress assay at the frequency and intensity used here. It is possible that the other GPCRs are mechanosensitive, and higher levels of shear stress or other forms of mechanical forces are required for their activation. Nevertheless, we could not find evidence in the literature that direct mechanical stimulation, rather than osmotic stress, can activate any of the aforementioned GPCRs to induce immediate downstream events (*e.g.*, PIP₂ deletion, change in intracellular calcium levels, etc.). However, AGTR1 and other GPCRs are proposed to be sensitive to membrane stretch when assayed indirectly by electrophysiological recording from HEK cells co-expressing TRPC6 (Mederos y Schnitzler et al., 2008).

How does GPR68 sense shear stress? There are reports of BDKRB2 activation by shear stress (Chachisvilis et al., 2006). Using time-resolved fluorescence microscopy and GPCR conformation-sensitive FRET, conformational dynamics of the receptor was detected upon application of fluid shear stress. This suggests that GPCRs can undergo conformational changes under fluid shear stress. GPR68 likely interacts with cytoskeleton to effectively sense and transduce tension, as the tensegrity model predicts that mechanical behavior of cells emerges by interactions among different cytoskeletal filaments and extracellular adhesions (Wang et al., 2001). It is also possible that an unknown upstream mechanosensor can activate GPR68; however, this factor would be expressed quite ubiquitously.

Role of GPR68 in endothelial cells

It is interesting that both Piezo1 and GPR68 are expressed in endothelial cells. However, we did not detect Piezo1 activation by calcium imaging upon laminar flow (Figure 4K), although Piezo1-dependent calcium transients were recorded in response to disturbed shear stress. This difference could be due to the fast inactivation of Piezo1 when heterologously expressed. Unlike Piezo1, activation of Gpr68 causes a robust calcium release from intracellular stores in response to both laminar and disturbed flows. Importantly, Gpr68-dependent mechanoresponses are present in MDA-MB-231, even when Piezo1 is knocked down, indicating that the two can function independently (Figure 2D). Indeed, Piezo1 is required for embryonic arterial remodeling and its deletion causes embryonic lethality, while Gpr68-deficient mice survive to adulthood and are grossly normal (Li et al., 2009b). Given that Piezo1 has also been recently implicated to play a role in FMD (Wang et al., 2016), as well as flow-stimulated vasoconstriction through endothelium-smooth muscle coupling (Rode et al., 2017), it is possible that both Piezo1 and Gpr68 contribute to sensing shear stress within endothelial cells. Analysis of double knockout mice could shed light on whether Piezo1 and Gpr68 play additive/overlapping roles in endothelial cells.

GPR68 can also be activated by protons. Low pH and shear stress are both relevant stimuli that endothelial cells experience *in vivo*. Both acidosis (blood pH~7.0) and shear stress cause acute vasodilation (Lindauer et al., 2003; Niebauer and Cooke, 1996), raising the possibility that GPR68 could be a polymodal receptor for the two distinct stimuli. Coincidence activation of GPR68 by proton and shear stress could endow GPR68 with the capacity to generate complex responses to these two physiologically relevant stimuli.

As a $G_{q/11}$ -coupled receptor, GPR68 activation is expected to lead to the cleavage of PIP_2 into IP_3 and DAG by PLC, and induces calcium release from the store. In endothelial cells, this could trigger several acute signaling pathways, including the activation of Ca^{2+} -gated channels (Orai1, $K_{Ca2.3}$, $K_{Ca3.1}$) or synthesis of NO by NOS or release of EDHF (Grgic et al., 2009). Depletion of membrane-bound PIP_2 may also activate KCNK channels and lead to the hyperpolarization of the cells (Pathan and Rusch, 2011). The release of NO, EDHF and activation of KCNK channels in turn can lead to hyperpolarization of smooth muscles surrounding the vessels, causing them to relax and therefore dilate the vessels. We have shown that NO is likely to be an essential downstream pathway of GPR68 and leads to vasodilation (Figure S4C). Future studies might reveal additional pathways that could be activated by GPR68.

Role of GPR68 in shear stress sensing *in vivo*

We demonstrate that GPR68 is essential for Flow-mediated dilation (FMD) *ex vivo*, and Flow-mediated outward remodeling (FMR) of small arteries *in vivo*. FMD is an acute dilatory response of the endothelium involved in tissue perfusion when the blood flow rate rises with increase in metabolic demand (Joyner and Casey, 2015; Levy et al., 2008). However, FMD does not necessarily correlate with systemic blood pressure. Indeed, in several mouse models without vimentin (Henrion et al., 1997) or dystrophin (Loufrani et al., 2001), FMD is selectively reduced with little change in blood pressure. Regardless, compromised flow-mediated dilation is considered to be a sign of endothelial dysfunction as observed in diseases related to vascular function. Given the requirement of GPR68 for FMD, it would be interesting to test whether the GPR68-deficient mice are prone to develop preclinical equivalent of hypertension, obesity or diabetes when challenged.

FMR is governed by the rise in shear stress exerted on the endothelial cells and leads to the outward growth of the vascular wall and increased diameter so that shear stress is normalized over time. FMR plays a major role in collateral artery growth, or arteriogenesis, which is crucial to improve collateral circulation and tissue perfusion in patients with ischemic diseases. FMR becomes progressively reduced in aging (Dumont et al., 2008), is decreased even earlier in rat models of hypertension (Tuttle et al., 2002) and diabetes (Freidja et al., 2012), and has a strong prognostic significance in patients (Lynch et al., 2012). New therapeutics that improve FMR would potentially bring significant benefit to patients suffering severe ischemia as this would accelerate collateral artery growth and thus reperfusion (Silvestre et al., 2013).

Role of GPR68 in other cells

GPR68 is also expressed in a few other cell types, including neurons in the brain and DRG and in leukocytes. We detected murine Gpr68 RNA in a subset of DRG neurons by *in situ* hybridization (data not shown). However, it is unlikely that Gpr68 is the sensor underlying the mechanically-activated currents observed in DRG neurons. All mechanically-activated currents in DRG neurons have fast sub-millisecond onset (Delmas et al., 2011). In comparison, the fastest-signaling GPCR described to date are the ones involved in photosensing, which require tens of millisecond to activate and to couple to downstream ion channels (Burns and Pugh, 2010). Gpr68 could serve as a modulator of other ion channels in DRG, similar to muscarinic acetylcholine receptors that modulate inward-rectifying K⁺ channels (Chuang et al., 1997). Gpr68 is also highly expressed in immune cells. It has been suggested that the expression of Gpr68 in myeloid-derived cells is required for prostate cancer cell-induced immunosuppression (Yan et al., 2014). GPR68 mice also have impaired T cell responses associated with a reduced frequency and number of dendritic cells (DCs), higher production of nitric oxide by macrophages, and defect in DCs migration to draining lymph nodes (Aoki et al., 2013; D'Souza et al., 2016). There's also evidence suggesting that GPR68 could be involved in recall of fear conditioning in mice (Huang et al., 2015). Interestingly, it is suggested that GPR68 as a proton sensor is required for proper enamel formation in humans although the KO mice lack the enamel formation phenotype (Parry et al., 2016). The mechanism of these effects, and whether mechanotransduction is involved in these various processes, is not clear.

Significance of the high throughput mechanical assay system and identification of GPR68

Our high throughput shear stress stimulation system vastly improves the throughput of mechanotransduction assays. This enabling technology has made unbiased, genome-wide screen for novel mechanosensitive proteins and pathways feasible. The identification of GPR68 as a novel mechanosensor validates the value and potential of this innovative system, and expands the repertoire of membrane proteins that sense mechanical forces *in vivo*.

CONTACT FOR REAGENTS AND RESOURCES SHARING

Further information and requests for resources and reagents should be directed to and will be fulfilled by the Lead Contact, Ardem Patapoutian (ardem@scripps.edu).

EXPERIMENTAL MODEL AND SUBJECT DETAILS

Animals—All procedures involving animal handling were approved by Institutional Animal Care and Use Committees (IACUC) of Genomics Institute of the Novartis Research Foundation (GNF), The Scripps Research Institute (TSRI) and CNRS Angers University. In addition, FMD and FMR experiments were performed in agreement with the guidelines from Directive 2010/63/EU of the European Parliament on the protection of animals used for scientific purposes.

Gpr68 knockout mice breeders (*Gpr68*^{tm1.1Yaxu}, C57BL/6J background, MGI ID: 3849457) were provided by Dr. Yan Xu (Indiana University School of Medicine). *Gpr68-eGFP* reporter mice (Tg(*Gpr68-EGFP*)IU33Gsat/Mmucd, RRID:MMRRC_031057-UCD) were purchased from GenSat Project from The Rockefeller University. All animals were in specific pathogen-free environment at GNF, TSRI and CNRS Angers University. They were housed in a 12 h light/dark cycle (light from 6 AM to 6 PM local time) in a temperature-controlled room (24 °C) with free access to food and water. All mice were not involved in procedures and are drug and test naïve. *Gpr68* knockout colony was maintain with Het × Het mating scheme and *Gpr68-eGFP* colony was maintain with het × WT scheme. 3 to 5 month-old male mice were used in the experiments with wild type male littermates as controls as required.

Cell lines and cell culture—HEK-293T cells were grown in Dulbecco's modified Eagle's medium containing 4.5 mg/ml glucose, 10% fetal bovine serum, 1× antibiotics/antimycotics. The human cell lines used in screening for shear stress-sensitive ones are purchase from American Type Culture Collection (ATCC) and Japanese Collection of Research Bioresources (JCRB) Cell Bank as a part of National Cancer Institute 60 Cancer Cell Panel (NCI-60). The cell lines were maintained in ATCC recommended media and conditions. Detailed culture information could be found on <http://www.atcc.org> by searching for catalog numbers of the cell line (listed in **KEY RESOURCES TABLE**). Cell line authentication information was supplied by ATCC. We were not able to obtain information on the sex of the cell line that are discontinued by vendors. The mouse primary endothelial cells are isolated from male *Gpr68* KO and *Gpr68-eGFP* mice age 3-5 months. Cells were cultured in Endo-PM media (Navone et al., 2013) on laminin / fibronectin coated plates (BD Biosciences) at 37 °C, 5% CO₂, with media changes every 2 days.

METHODS DETAILS

Constructs and Compounds—Human GPR68, GPR132, AGTR1, AVPR1A, BDKRB2, CHRM5, EDNRA, HRH1, PTHR1 were purchase from Missouri S&T cDNA Resource Center. Mouse Gpr68 in pCDNA3.1 was from Novartis internal collection. Expression constructs of human GPR68 and mouse Gpr68 were sub-cloned into pIRES2-EGFP vector by inserting the coding sequence (CDS) of genes at EcoRI and BamHI sites. The final CDS of human GPR68 in the constructs was the following:

```
ATGGGGAACATCACTGCAGACAACTCCTCGATGAGCTGTACCATCGACCAT
ACCATCCACCAGACGCTGGCCCCGGTGGTCTATGTTACCGTGCTGGTGGTG
GGCTTCCCGGCCAACTGCCTGTCCCTCTACTTCGGCTACCTGCAGATCAAG
GCCCCGAACGAGCTGGGCGTGACCTGTGCAACCTGACGGTGGCCGACCT
CTTCTACATCTGCTCGCTGCCCTTCTGGCTGCAGTACGTGCTGCAGCACGA
CAACTGGTCTCACGGCGACCTGTCTGCCAGGTGTGCGGCATCCTCCTGTA
CGAGAACATCTACATCAGCGTGGGCTTCCTCTGCTGCATCTCCGTGGACCG
CTACCTGGCTGTGGCCCATCCCTTCCGCTTCCACCAGTTCCGGACCCTGAA
GGCGGCCGTCGGCGTCAGCGTGGTCATCTGGGCCAAGGAGCTGCTGACCA
GCATCTACTTCCTGATGCACGAGGAGGTCATCGAGGACGAGAACCAGCACC
GCGTGTGCTTTGAGCACTACCCCATCCAGGCATGGCAGCGCGCCATCAACT
ACTACCGCTTCCTGGTGGGCTTCCTCTTCCCCATCTGCCTGCTGCTGGCGTC
CTACCAGGGCATCCTGCGCGCCGTGCGCCGGAGCCACGGCACCCAGAAGA
GCCGCAAGGACCAGATCCAGCGGCTGGTGCTCAGCACCGTGGTCATCTTCC
TGGCCTGCTTCCTGCCCTACCACGTGTTGCTGCTGGTGCGCAGCGTCTGGG
AGGCCAGCTGCGACTTCGCCAAGGGCGTTTCAACGCCTACCACTTCTCCC
TCCTGCTCACCAGCTTCAACTGCGTCGCCGACCCCGTGCTCTACTGCTTCG
TCAGCGAGACCACCCACCGGACCTGGCCCGCCTCCGCGGGGCTGCTG
GCCTTCCTCACCTGCTCCAGGACCGGCCGGGCCAGGGAGGCCTACCCGCT
GGGTGCCCCCGAGGCCTCCGGGAAAAGCGGGGCCAGGGTGAGGAGCCC
GAGCTGTTGACCAAGCTCCACCCGGCCTTCCAGACCCCTAACTCGCCAGGG
TCGGGCGGGTTCCCCACGGGCAGGTTGGCCTAG
```

The final CDS of mouse Gpr68 in the constructs was the following:

```
ATGGGGAACATCACTACAGAAAACCTCCTCACTATCTTGCCCCATCGACCAC
ACCATCCACCAGACACTAGCCCCAGTGGTCTATGTGACCGTGCTGGTGGTG
GGCTTCCCAGCCAACTGCCTGTCCCTCTACTTCGGGTACTTGAGATCAAG
GCCCCGAATGAGCTGGGAGTGACCTGTGTAACTGACCATGTCAGACCTG
TTCTATATCTGTTCACTTCCCTTCTGGCTGCAGTACGTGCTTCAGCACGACG
ACTGGTCCCATGGTGACCTATCCTGCCAGGTGTGTGGCATCCTCCTCTATGA
GAACATTTACATCAGCGTGGGCTTCCTCTGCTGCATCTCCATCGACCGCTAC
CTGGCTGTGGCCACCCCTTCCGCTTCCACCAGTTCCGCACCCTGAAGGCA
GCCGTGGGTGTCAGTGTGCTCATCTGGGCCAAGGAGCTGCTGACCAGCAT
CTACTTCCTCAATCACAAGGAGGTCATTGAGGACGAGGACCAGCACCAGGT
CTGCTTTGAGCATTACCCTATCCAGGCCTGGCAGCGTAGCATCAACTACTAC
CGCTTCCTGGTGGGCTTCTCTTCCCCATCTGCCTGCTGCTGGCCTCCTACC
AGGGCATCCTGCGGGCTGTGCGCCGACGCCACGGCACACAGAAGAGCCGC
```

AAGGACCAGATTCAGCGGCTGGTGCTCAGCACCGTGGTCATCTTCCTGGCT
 TGCTTTCTACCTACCACGTGCTGCTGCTGGTACGCAGCCTCTGGGAGAGA
 AACTGTGAGTTTGCCAAGAGCATCTTCAACGTCTATCACTTCTCCCTCCTCC
 TCACCAGCTTCAACTGTGTAGCTGACCCGGTGCTGTACTGCTTTGTCACTG
 AGACCACTCACAGGGACCTAGCCCCGCTCCGAGGAGCCTGCCTAGCTGTCC
 TTACCTGCTCTAGGACAAGCAGGGCCAGGGAGGCCTACCTCTGGGTGCCC
 CTGAGGCCTCTGGGAAAAGTGGGGCCCAGGGCGAGGAACCTGAATTGTTA
 ACCAAGCTCCACTCAGCCTTCCAGACCCCTAGCTCACTGGGAGTGGGAGG
 GCCCTCCACAGTGGGGTTGGCCTAG

Constructs of mouse Piezo1 and rat TrpV4 were described previously (Coste et al., 2010; Liedtke et al., 2000). Briefly, a 7.644 kb fragment of mouse Piezo1 CDS was amplified from cDNA libraries generated from Neuro2A total RNA using primers mPiezo1 fwd (5' atggagccgcacgtgctg 3') and mPiezo1 rev (5' ctactccctctcacgtgtcca 3') and cloned into pcDNA3.1(-) (Invitrogen) with NotI and HindIII restriction sites. A cDNA encoding TRPV4 was amplified from a rat kidney RNA library and cloned in pcDNA3.1 (-). All constructs were fully sequence verified. Agonists for the human GPCRs listed above and the PLC inhibitor U73122 were purchased from Tocris Bioscience. Ogerin (ZINC67740571) was synthesized by WuXi AppTek as a part of contract research services. The structure of Ogerin was described previously (Huang et al., 2015).

Engineering

a. Construction of the high-throughput shear stress stimulation system: The high-throughput disturbed flow system utilizes a 384-pin array printed by Projet MJP 3500 (3D Systems) using UV-cured Visijet Crystal resin (3D Systems). The circular face of the pin is 2.8mm in diameter. A square diaphragm neodymium subwoofer driver (W3-1750S, Tang Band) is used as the driver. A miniature 3-axis accelerometer (ADXL326, Analog Devices) affixed to array monitors the motion of the array. The assembly sits on a machined aluminum assay plate guide. Shims and set screws are employed to accurately align the array with the assay plate. A custom interface is written using LabView (National Instruments) which allows the user to set frequency, amplitude and duty cycle of the stimulation. The signal is sent to an amplifier (D-150A II, Crown) to drive the pin and create fluid motion. The accelerometer signal is acquired by a data acquisition card (USB-6341, National Instruments) and instantaneously displayed in LabView for the user to monitor the motion of the pin array.

b. Estimation of the shear stress intensity: The particle image velocimetry method used for estimating the shear stress intensity on the bottom of the assay well was described previously (Ranade et al., 2014). Briefly, we dispensed a suspension of 6 μ m-diameter Texas Red fluorescent beads (Life Technologies) into the imaging chamber and let them settle to the bottom. We applied sine wave stimulations at 60Hz and imaged the motion of the beads at 500 frames per second using ORCA-Flash 4.0 CMOS camera (Hamamatsu). Images were analyzed using NIS-Elements (Nikon) and velocity values of ~60 beads were averaged for each input power setting. We calculated shear stress intensity at 3 μ m above the surface of

the cover slip as an approximation of that experienced by the cells cultured on the surface of the cover slip.

Cell-based Experiments

a. FLIPR assays: FLIPR experiments were performed as previously described (Ranade et al., 2014). Before loading, the cells were washed with assay buffer (1× HBSS with calcium and 10 mM HEPES, pH adjusted to 7.4) using ELx405 CW plate washer (BioTek). Cells were loaded with Fluo-3 for 60 min (4 μM Fluo-3, 0.04% F-127 in assay buffer) at 37 °C. Cells were washed again with assay buffer and the plates were centrifuged at 15 g for 5 s before assayed on FLIPR Tetra (Molecular Devices). The data was analyzed on Screenworks 3.1 (Molecular Devices) by calculating the difference between the maximum and minimum fluorescence intensity during the course of recording, then normalize to the starting fluorescence intensity:

$$\text{Fold of Response} = (F_{\text{max}} - F_{\text{min}}) / F_{\text{start}}$$

b. Disturbed shear stress stimulation: When applying shear stress with high-throughput disturbed flow system, we first thoroughly dry the pin array with compressed air then mounted the 384-well plate on the system. Two stimulation protocols were used. The short protocol applies stimulation for 4 s at 60 Hz, and the long protocol applies 0.2 s pulses at 60 Hz every 2 s for 40 s. After each assay, the pin array was washed thoroughly with distilled water and air dried before mounting onto the next plate. Whenever compounds were used, to avoid carry-over, the array was first thoroughly washed with 70% EtOH, then with distilled water and dried before assaying the next plate.

c. Laminar shear stress stimulation: HEK-293T cells were plated in the Collagen IV-coated μ-slide I 0.4 laminar flow chambers (Ibidi) 24 h prior to experiments. After loading Fura-2, the chambers were mounted onto the microscope and connected to the Ibidi perfusion pump. Cells were given pulsatile (1 Hz) or continuous laminar flow for 120 s.

d. Plasmid DNA and siRNA transfection: For DNA plasmid transfection with HEK-293T cells in poly-D-Lysine coated 384-well assay plates (Greiner Bio-One), we use 65 ng plasmid, 0.195 μl Eugene 6 (Roche) and 1×10^4 cells in 40 μl standard growth medium for each well. When transfecting HEK-293T cells on poly-D-Lysine glass cover slips (BD Biosciences), we use 500 ng of plasmids, 1.5 μl Eugene 6 and 1×10^5 cells in 600 μl growth medium. For laminar flow chamber experiments, cells were first transfected in 24-well plate in the same condition. 24 h later they were trypsinized and plated in μ-slides I 0.4 flow chambers (Ibidi). Cells were assayed 48 h post-transfection.

For siRNA transfection in 384-well plates, we mixed 1 pmol siRNA with 20 μl Opti-MEM and 0.15 μl Lipofectamine RNAiMax (Life Technologies) in each well, incubated for 20 min at room temperature, then added 20 μl cells (6×10^3 cells per well for MDA-MB-231, 1×10^4 cells per well for HeLa). When transfecting siRNA on glass coverslips, 20 pmol siRNA, 1 μl RNAiMax and 100 μl Opti-MEM were mixed and incubated for 20 min, then mixed with

500 μ l cells (1×10^5 cells per well for HeLa, 2×10^5 cells per well for early passage HUVECs). SiRNAs were from Dharmacon. Cells were assayed 72h post-transfection.

e. Calcium imaging: Fura-2 single cell calcium imaging was performed as previous described (Ranade et al., 2014). Briefly, cells were seeded onto poly-D-Lysine cover slips (BD Biosciences). We loaded the cells with the ratiometric Ca^{2+} indicator Fura-2 AM (ThermoFisher) in imaging buffer ($1 \times$ Hanks Balanced Salt Solution (HBSS) and 10 mM HEPES, pH adjusted to 7.4 by NaOH). After 30 minutes of loading at room temperature, cover slips were washed with imaging buffer and then mounted onto the disturbed shear stress imaging chamber and assayed at room temperature. The intracellular Ca^{2+} concentration was expressed as the 340/380 ratio.

f. High-throughput siRNA screen: To assemble a set of arrayed siRNAs targeting genes encoding multi-pass transmembrane (MPTM) proteins, we subjected 34,226 non-identical protein sequences extracted from the August 21, 2011 version of Human Refseq to sequence-based membrane topology and signal peptide prediction using the Phobius algorithm and website, identifying 2,907 human genes encoding one or more MPTM proteins (Kall et al., 2004, 2007). An unconstrained prediction model was employed, signal peptides annotated where predicted, and all two-pass or more predictions collapsed from protein to gene space to ensure that no siRNAs targeting non-MPTM protein isoforms were excluded. The siRNA library was picked from a genome-wide siRNA library and arrayed in 384-well poly-D-Lysine coated assay plate with one single oligo in each well (63 plates in total). MDA-MB-231 cells were transfected with the siRNA using a robotic liquid handler and incubated in a robot-assisted incubator (GNF Systems). Cells were assayed after 72h with HT disturbed shear stress system. Wells with calcium signal $3 \times$ standard deviations below the plate mean were considered as hit wells. Genes with more than 3 hit wells were considered hits. We then crosschecked the bioinformatics results and the literature to filter out the hits that have known functions unrelated to acute (second-scale) calcium signaling. We picked the siRNA against hit genes from primary screen from the original genome-wide library and carried out a reconfirmation screen. For final screen, we purchased smartpool siRNA (Dharmacon OTP siRNAs, GE Healthcare) against the hits from the reconfirmation screen. For controls, in addition to PIEZO1 siRNA, we also included siRNA against a SERCA Ca^{2+} -ATPase (ATP2A2) to control for the effect of intracellular calcium store.

g. Real-time pH measurement: 2',7'-Bis(3-carboxypropyl)-5(6)-carboxyfluorescein (BCEFC) was selected as pH indicator based on its dynamic range (pH6~pH8), which fits GPR68 activation range best among all pH-sensitive dyes. BCECF increase fluorescence when pH increases. Free BCECF was used to monitor extracellular pH and its cell-permeable acetoxymethyl (AM) ester version was used for monitoring intracellular pH. Cells in assay plates were first washed with HBSS-pH7.4 on an ELx405 CW plate washer (BioTek). BCECF was then incubated with cells for 1 h at 37 °C. When measuring intracellular pH, cells were then washed with HBSS-pH7.4 again. When measuring extracellular pH, no wash step was added. Fluorescence was read on FLIPR for 10s and acid or base were added to the buffer to shift pH to various final values from pH6.1 to pH8.3, while fluorescence was continuously monitoring for additional 150 s. For shear stress

stimulation, fluorescence was recorded for 10s and disturbed flow was applied for 60 s. Data was analyzed by ScreenWorks 3.0 (Molecular Devices) by exporting the real-time fluorescence values of the recordings corresponding to each treatment.

h. Fluorescence-activated Cell Sorting: Spleens from Gpr68 eGFP reporter mice were isolated and dissociated in FACS buffer (PBS containing 2% FBS and 2 mM EDTA) and red blood cells were lysed using RBC Lysis Buffer (eBioscience). Samples were washed once in FACS buffer, filtered through 100 μ m diameter nylon mesh, and incubated with FcBlock (BD Biosciences) for 5 minutes at room temperature. They were then stained with BV421 CD4 (Biolegend), BV650 CD3 (Biolegend), APC-Cy7 CD19 (Biolegend), PerCP-Cy5.5 CD8 (BD Biosciences), and APC NK1.1 (eBioscience) for 20 min at 4 °C in the dark. The cells were washed once then resuspended in FACS buffer. Data was acquired using a LSRII flow cytometer (BD Biosciences) and was analyzed using Flowjo (Treestar). Populations were defined as follows: CD4T cells: CD3⁺ CD4⁺ CD8⁻, CD8T cells: CD3⁺ CD8⁺ CD4⁻, B cells: CD3⁻ NK1.1⁻ CD19⁺, NK cells: CD3⁻ NK1.1⁺ CD19⁻. For cell sorting, spleens were processed and stained as above, but were sorted using a FACS Aria II Cell sorter (BD Biosciences) into Trizol LS (ThermoFisher) and processed as previously described.

i. RNA sequencing of mouse bladder MVECs: The Gpr68 eGFP reporter mice were sacrificed with CO₂ and the bladders were dissected out and cut into small pieces with micro scissors in PBS. The tissues were digested with 12.5 mg/mL collagenase IV (ThermoFisher) and 10 U/mL papain (Worthington) at 37 °C for 1 h. The suspension was triturated with fire-polished glass pipettes and then spun down to collect the cell pellet. After washing the pellet twice with PBS, the cells were suspended in FACS buffer. The cells were stained with CD31-APC and CD45-APC-Cy7 (BD Biosciences) for 20 min at 4 °C in the dark, and stained with PI before sorting. We sorted the cells that are CD31⁺ CD45⁻ GFP⁺ and CD31⁺ CD45⁻ GFP⁻ into two 1.5 mL tubes each containing 1ml Trizol LS (ThermoFisher). Total RNA was extracted and column purified using RNeasy kit (Qiagen). For each condition, 10ng of total RNA was used to produce the cDNA libraries using Ovation RNA-Seq System V2 (NuGEN). The cDNA was then fragmented to ~200bp size range and prepared for RNA Sequencing by Ovation Ultralow DR Multiplex System (NuGEN) and the quality validated using High Sensitivity DNA Kit (Agilent Technologies). cDNA libraries were run on a HiSeq 1000 (Illumina) with 50 bp single-end reads. Reads were de-multiplexed with the Illumina pipeline. Raw reads were aligned to a reference FASTA file which contains a curated list of mouse transcripts, plus mitochondrial sequence, and mitochondrial transcripts, and Illumina adaptor sequences. Alignment was done with BWA (Burrows-Wheeler Aligner) (Li and Durbin, 2009) and RPKM values were created from the SAM output file (Li et al., 2009a). All samples contained at least 20 million mapped reads. Messenger RNAs less than 200 bp were eliminated from analysis.

j. Culturing of mouse primary cerebral MVECs: Whole cerebrum from Gpr68-eGFP reporter mice were isolated in cold PBS and homogenized in buffer containing 1× HBSS, 15mM HEPES and 1% dextran sulphate on ice. Equal volumes of 26% dextran sulphate was mixed well with the homogenized samples and centrifuged at 5800g at 4 °C for 10 min. The pellet was resuspended in 0.625mg/mL Liberase enzyme mix (Millipore Sigma) and

digested at 37 °C for 1hr (triturate once every 30 min using fire-polished glass pipette). Digestion was then stopped with cold isolation buffer and spun down. The pellet was resuspended in 25% BSA and spun for 15 minutes at 1500rpm at room temperature. The final pellet was resuspended in Endo-PM media (Navone et al., 2013) and plated onto laminin / fibronectin coated culture plates. Cells were cultured for at 37 °C, 5% CO₂ until confluent with media changes every 2 days.

k. Lentiviral shRNA knockdown and laminar flow stimulation of MVECs: Dharmacon TRC shRNA constructs for murine Gpr68 were purchased from GE Healthcare. Gpr68 shRNA constructs were co-transfected with first generation packaging vectors using Lipofectamine 2000 (Life Technologies) according to the manufacturer's instructions into HEK293T cells. Medium was changed after 24hrs and the supernatant was collected 48hrs after transfection. We centrifuged the supernatant at 500 g for 10 min and added over cultured primary endothelial cells (400 µL of supernatant per well on 24-well plate). 24hrs after infection medium was replaced with Endo-PM containing 2 µg/mL puromycin. 48h post infection, the MVECs were gently dissociated using Trypsin (Lonza) and plated in µ-slide I 0.2 laminar flow chamber (Ibidi) and kept in Endo-PM with 2 µg/mL puromycin. 72 h later, cells were loaded with Fura-2 and calcium imaging experiments were conducted with pulsatile laminar flow (1Hz) stimulation.

***In Vivo* Experiments**

a. Mesenteric arteries cannulation: 1st, 2nd and 3rd arterial segments were isolated from the mesenteric circulation and cannulated at both ends on glass micro-cannulae and mounted in a video-monitored perfusion system (Living System, LSI, Burlington, VT). Arterial segments were bathed in a 5 ml organ bath containing a physiological salt solution (PSS) of the following composition (in mM): 135.0, NaCl, 15.0, NaHCO₃, 4.6 KCl, 1.5, CaCl₂, 1.2, MgSO₄, 11.0, glucose, 10.0, N-2-hydroxyethylpiperazine-N-2-ethylsulfonic acid. The PSS was maintained at pH7.4, PO₂ 160 mmHg, PCO₂ 37 mmHg. Perfusion of arterial segments was obtained with 2 peristaltic pumps, one controlling flow rate and one under the control of a pressure-servo control system. Pressure at both ends of the arterial segment was monitored using pressure transducers. Arterial contractility was assessed with KCl (80 mM) and phenylephrine 1 µmol/L. Endothelium integrity was assessed with acetylcholine (1 µM) after precontraction with phenylephrine (50% of maximum contraction). Pressure was then set at 75mmHg and flow was increased by step (3 to 50 µl per min) through the distal pipette with a peristaltic pump. Arteries were then bathed in a Ca²⁺-free PSS containing ethylene-bis-(oxyethylenenitrolo) tetra-acetic acid (2 mmol/L) and sodium nitroprusside (10 µmol/L). Pressure was then increased by step from 10 to 125 mmHg, in the absence of flow, in order to determine passive arterial diameter (Henrion et al., 1997).

b. Flow-mediated outward remodeling of resistance arteries: 4-5-month old GPR68 KO and WT mice were submitted to surgery in order to increase blood flow in mesenteric artery as previously described (Caillon et al., 2016). Briefly, 3 consecutive first-order mesenteric arteries were used. Ligatures were applied to second-order branches as shown on Figure 7C. The artery located between the two ligated arteries was designed as high flow (HF) artery. Arteries located at distance of the ligated arteries were used as control (normal flow, NF). In

this protocol, animals were anesthetized with isoflurane (2.5%). They were treated with buprenorphine (Temgesic; 0.1 mg/kg, s.c.) before and after surgery.

Mice were sacrificed after 14 days before collection of HF and NF first order arteries and of the corresponding HF and NF third order mesenteric arteries. Their passive diameter was then measured using pressure arteriography as describe above.

c. Blood pressure radiotelemetry: Pressure radio transmitters (HD-X11, Data Science International) were implanted into left carotid artery according to Manufacturer's recommended procedure. Blood pressure and heart rate were recorded continuously and exported as 5-minute segments. Baseline blood pressure and heart rate data was averaged from last day of baseline measurements of all cohorts (usually 3rd or 4th day after the start of recording to obtain consistently stable measurements).

d. Ultrasound echocardiography: Mice were continuously anesthetized by 0.8–1% isoflurane (mixed with 1 L/min 100% O₂) inhalation and immobilized on a heating platform to maintain the body temperature at 37°C ± 0.5°C. Heart rate (HR) and respiratory physiology were continuously monitored by ECG electrodes. They were analyzed by B-mode and M-mode echocardiography using Vevo3100 with a 40 MHz transducer (VisualSonics). All M-mode measurements were performed in end-diastole and end-systole. End-diastolic and end-systolic measurements were obtained at the time of maximal internal chamber dimensions and at the minimal internal chamber dimensions, respectively. The LV structural parameters measured from short axis view in M-mode were used in the calculation of LV ejection fraction (EF) and LV fractional shortening (FS).

Miscellaneous

a. Quantitative reverse transcriptase PCR: For tissue qPCR, DRG were freshly isolated from adult C57BL/6J wild type mice and snap frozen on dry ice and total RNA was isolated using Trizol/choloform method. Total RNA from all other tissues was purchased from Zyagen. For qPCR using cultured cells, samples were lysed with Trizol and total RNA was isolated using chloroform/isopropanol precipitation. 100-200ng of total RNA was used to generate cDNA using the Quantitect Reverse transcript kit (Qiagen). Real time Taqman PCR assays for mouse and human Gpr68 were purchased from Life Technologies (assay id: Mm 00558545_s1 and Hs 00268858_s1) and IDT (Mm.PT.58.42531755 and Hs.PT.58.27651490.g) with a FAM reporter dye and a non-fluorescent quencher.

We used FastStart Universal probe master mix (Rox) (Roche). The reaction was run in the 7900HT fast real time system (ABI) using 0.5ul of the cDNA in a 10ul reaction according to the manufacturer's instructions in triplicate. Calibrations and normalizations were done using the 2^{-CT} method (Livak and Schmittgen, 2001), where $CT = ((CT(\text{target gene}) - CT(\text{reference gene})) - (CT(\text{calibrator}) - CT(\text{reference gene})))$. Gapdh and b-actin were used as the reference genes.

b. Immunostaining: For GFP immunostaining experiments, tissues from various organs were collected from 7-week-old wild type and Gpr68 eGFP reporter mice after perfusion with 4% PFA. Tissues were briefly fixed in 4% PFA and were dehydrated through an ethanol

series/xylene and embedded in paraffin. 5µm sections were cut and incubated with blocking solution containing 1× PBS, 10% blocking serum, 3% BSA and 0.4% Triton× 100 for 1hr at room temperature. Slides were stained overnight with a goat anti-GFP antibody (Lifespan Biosciences). Slides were treated with Omni-Map anti -goat secondary antibody conjugated with HRP (Ventana) followed by development using the Chromo Map DAB kit (Ventana). Slides were mounted with Cytoseal and scanned using the Nanozoomer 2.0 HT (Hamamatsu).

We tested murine Gpr68 antibodies from Lifespan Biosciences (LS-A3968 and LS-A1194) and antibodies custom generated at Pierce Biotechnologies (peptide sequences: RTSRAREAYPLGAPEASGK and EPELLTKLHSAFQTPSSLG). We determined that none of the above can specifically detect Gpr68 protein in HEK-293T cells overexpressing murine Gpr68 in our immunohistochemistry experiments.

c. In situ hybridization: Tissues from C57BL/6J mice were isolated after perfusion and fixed in 10% formalin overnight. The tissues were dehydrated through an ethanol series/ xylene and embedded in paraffin. 10µm sections were cut and in situ hybridization was carried out using the RNAscope assay (ACD Bio). Development of signal was done using the RNAscope 2.0 HD brown detection kit. Probes for mGpr68 (cat. #: 319321) and DapB negative control (cat #: 310043) were purchased from Advanced Cell Diagnostics. Slides were mounted with Cytoseal and scanned using the Nanozoomer 2.0 HT (Hamamatsu).

QUANTIFICATION AND STATISTICAL ANALYSIS

Unless otherwise noted in Results and Figure Legends, statistical significance was evaluated using unpaired two-tailed Students's t test when comparing the difference between two samples, and one-way ANOVA was employed when comparing the samples among groups with more than two samples. All data plotted as mean ± SEM. For experiments that includes samples taken from animals, n represent the number of animals used in the analysis.

DATA AND SOFTWARE AVAILABILITY

RNAseq data of Gpr68-eGFP endothelial cells discussed in this publication have been deposited in NCBI's Gene Expression Omnibus and are accessible through GEO Series accession number GSE111784 (<https://www.ncbi.nlm.nih.gov/geo/query/acc.cgi?acc=GSE111784>)

Supplementary Material

Refer to Web version on PubMed Central for supplementary material.

Acknowledgments

We thank Alec Wilson for engineering support; Sungjoon Kim for supplying human cancer cells; Craig Mickanin for picking the siRNA library; Yufeng Zhai and Yingyao Zhou for help with siRNA screen data analysis; Zhaozhu Qiu, Matt Petrus, Buu Tu, Loren Miraglia, Sanjeev Ranade, Angelica Romero, Glenn Federe, James Watson, Teri Johnson, Rita Moran and Kathryn Spencer for assistance; and members of Patapoutian group for constructive discussions. This work was partly supported by a grant from the NIH (NIH R01 #DE022358 to A.P.). A.P. is an investigator of the Howard Hughes Medical Institute.

References

- Aoki H, Mogi C, Hisada T, Nakakura T, Kamide Y, Ichimonji I, Tomura H, Tobo M, Sato K, Tsurumaki H, et al. Proton-sensing ovarian cancer G protein-coupled receptor 1 on dendritic cells is required for airway responses in a murine asthma model. *PloS one*. 2013; 8:e79985. [PubMed: 24244587]
- Burns ME, Pugh EN Jr. Lessons from photoreceptors: turning off g-protein signaling in living cells. *Physiology*. 2010; 25:72–84. [PubMed: 20430952]
- Caillon A, Grenier C, Grimaud L, Vessieres E, Guihot AL, Blanchard S, Lelievre E, Chabbert M, Foucher ED, Jeannin P, et al. The angiotensin II type 2 receptor activates flow-mediated outward remodelling through T cells-dependent interleukin-17 production. *Cardiovascular research*. 2016; 112:515–525. [PubMed: 27328880]
- Chachisvilis M, Zhang YL, Frangos JA. G protein-coupled receptors sense fluid shear stress in endothelial cells. *Proceedings of the National Academy of Sciences of the United States of America*. 2006; 103:15463–15468. [PubMed: 17030791]
- Chen P, Zuo H, Xiong H, Kolar MJ, Chu Q, Saghatelian A, Siegwart DJ, Wan Y. Gpr132 sensing of lactate mediates tumor-macrophage interplay to promote breast cancer metastasis. *Proceedings of the National Academy of Sciences of the United States of America*. 2017; 114:580–585. [PubMed: 28049847]
- Chiu JJ, Chien S. Effects of disturbed flow on vascular endothelium: pathophysiological basis and clinical perspectives. *Physiological reviews*. 2011; 91:327–387. [PubMed: 21248169]
- Chuang H, Jan YN, Jan LY. Regulation of IRK3 inward rectifier K⁺ channel by m1 acetylcholine receptor and intracellular magnesium. *Cell*. 1997; 89:1121–1132. [PubMed: 9215634]
- Coste B, Mathur J, Schmidt M, Earley TJ, Ranade S, Petrus MJ, Dubin AE, Patapoutian A. Piezo1 and Piezo2 are essential components of distinct mechanically activated cation channels. *Science*. 2010; 330:55–60. [PubMed: 20813920]
- D'Souza CA, Zhao FL, Li X, Xu Y, Dunn SE, Zhang L. OGR1/GPR68 Modulates the Severity of Experimental Autoimmune Encephalomyelitis and Regulates Nitric Oxide Production by Macrophages. *PloS one*. 2016; 11:e0148439. [PubMed: 26828924]
- Delmas P, Hao J, Rodat-Despoix L. Molecular mechanisms of mechanotransduction in mammalian sensory neurons. *Nature reviews Neuroscience*. 2011; 12:139–153. [PubMed: 21304548]
- Driscoll M, Chalfie M. The mec-4 gene is a member of a family of *Caenorhabditis elegans* genes that can mutate to induce neuronal degeneration. *Nature*. 1991; 349:588–593. [PubMed: 1672038]
- Dumont O, Pinaud F, Guihot AL, Baufreron C, Loufrani L, Henrion D. Alteration in flow (shear stress)-induced remodelling in rat resistance arteries with aging: improvement by a treatment with hydralazine. *Cardiovascular research*. 2008; 77:600–608. [PubMed: 18006444]
- Ernstrom GG, Chalfie M. Genetics of sensory mechanotransduction. *Annual review of genetics*. 2002; 36:411–453.
- Freidja ML, Tarhouni K, Toutain B, Fassot C, Loufrani L, Henrion D. The AGE-breaker ALT-711 restores high blood flow-dependent remodeling in mesenteric resistance arteries in a rat model of type 2 diabetes. *Diabetes*. 2012; 61:1562–1572. [PubMed: 22415880]
- Grgic I, Kaistha BP, Hoyer J, Kohler R. Endothelial Ca⁺⁺-activated K⁺ channels in normal and impaired EDHF-dilator responses—relevance to cardiovascular pathologies and drug discovery. *British journal of pharmacology*. 2009; 157:509–526. [PubMed: 19302590]
- Henrion D, Terzi F, Matrougui K, Duriez M, Boulanger CM, Colucci-Guyon E, Babinet C, Briand P, Friedlander G, Poitevin P, et al. Impaired flow-induced dilation in mesenteric resistance arteries from mice lacking vimentin. *The Journal of clinical investigation*. 1997; 100:2909–2914. [PubMed: 9389758]
- Huang M, Chalfie M. Gene interactions affecting mechanosensory transduction in *Caenorhabditis elegans*. *Nature*. 1994; 367:467–470. [PubMed: 7509039]
- Huang XP, Karpiak J, Kroeze WK, Zhu H, Chen X, Moy SS, Sadoris KA, Nikolova VD, Farrell MS, Wang S, et al. Allosteric ligands for the pharmacologically dark receptors GPR68 and GPR65. *Nature*. 2015; 527:477–483. [PubMed: 26550826]

- Ishida T, Takahashi M, Corson MA, Berk BC. Fluid shear stress-mediated signal transduction: how do endothelial cells transduce mechanical force into biological responses? *Annals of the New York Academy of Sciences*. 1997; 811:12–23. discussion 23–14. [PubMed: 9186580]
- Jaalouk DE, Lammerding J. Mechanotransduction gone awry. *Nature reviews Molecular cell biology*. 2009; 10:63–73. [PubMed: 19197333]
- Joyner MJ, Casey DP. Regulation of increased blood flow (hyperemia) to muscles during exercise: a hierarchy of competing physiological needs. *Physiological reviews*. 2015; 95:549–601. [PubMed: 25834232]
- Kall L, Krogh A, Sonnhhammer EL. A combined transmembrane topology and signal peptide prediction method. *Journal of molecular biology*. 2004; 338:1027–1036. [PubMed: 15111065]
- Kall L, Krogh A, Sonnhhammer EL. Advantages of combined transmembrane topology and signal peptide prediction—the Phobius web server. *Nucleic acids research*. 2007; 35:W429–432. [PubMed: 17483518]
- Kang L, Gao J, Schafer WR, Xie Z, Xu XZ. C. elegans TRP family protein TRP-4 is a pore-forming subunit of a native mechanotransduction channel. *Neuron*. 2010; 67:381–391. [PubMed: 20696377]
- Levina N, Totemeyer S, Stokes NR, Louis P, Jones MA, Booth IR. Protection of Escherichia coli cells against extreme turgor by activation of MscS and MscL mechanosensitive channels: identification of genes required for MscS activity. *The EMBO journal*. 1999; 18:1730–1737. [PubMed: 10202137]
- Levy BI, Schiffrin EL, Mourad JJ, Agostini D, Vicaute E, Safar ME, Struijker-Boudier HA. Impaired tissue perfusion: a pathology common to hypertension, obesity, and diabetes mellitus. *Circulation*. 2008; 118:968–976. [PubMed: 18725503]
- Li H, Durbin R. Fast and accurate short read alignment with Burrows-Wheeler transform. *Bioinformatics*. 2009; 25:1754–1760. [PubMed: 19451168]
- Li H, Handsaker B, Wysoker A, Fennell T, Ruan J, Homer N, Marth G, Abecasis G, Durbin R, Genome Project Data Processing S. The Sequence Alignment/Map format and SAMtools. *Bioinformatics*. 2009a; 25:2078–2079. [PubMed: 19505943]
- Li H, Wang D, Singh LS, Berk M, Tan H, Zhao Z, Steinmetz R, Kirmani K, Wei G, Xu Y. Abnormalities in osteoclastogenesis and decreased tumorigenesis in mice deficient for ovarian cancer G protein-coupled receptor 1. *PloS one*. 2009b; 4:e5705. [PubMed: 19479052]
- Li J, Hou B, Tumova S, Muraki K, Bruns A, Ludlow MJ, Sedo A, Hyman AJ, McKeown L, Young RS, et al. Piezo1 integration of vascular architecture with physiological force. *Nature*. 2014; 515:279–282. [PubMed: 25119035]
- Li W, Feng Z, Sternberg PW, Xu XZ. A C. elegans stretch receptor neuron revealed by a mechanosensitive TRP channel homologue. *Nature*. 2006; 440:684–687. [PubMed: 16572173]
- Lindauer U, Vogt J, Schuh-Hofer S, Dreier JP, Dirnagl U. Cerebrovascular vasodilation to extraluminal acidosis occurs via combined activation of ATP-sensitive and Ca²⁺-activated potassium channels. *Journal of cerebral blood flow and metabolism: official journal of the International Society of Cerebral Blood Flow and Metabolism*. 2003; 23:1227–1238.
- Livak KJ, Schmittgen TD. Analysis of relative gene expression data using real-time quantitative PCR and the 2(-Delta Delta C(T)) Method. *Methods*. 2001; 25:402–408. [PubMed: 11846609]
- Loufrani L, Matrougui K, Gorny D, Duriez M, Blanc I, Levy BI, Henrion D. Flow (shear stress)-induced endothelium-dependent dilation is altered in mice lacking the gene encoding for dystrophin. *Circulation*. 2001; 103:864–870. [PubMed: 11171796]
- Ludwig MG, Vanek M, Guerini D, Gasser JA, Jones CE, Junker U, Hofstetter H, Wolf RM, Seuwen K. Proton-sensing G-protein-coupled receptors. *Nature*. 2003; 425:93–98. [PubMed: 12955148]
- Lukacs V, Mathur J, Mao R, Bayrak-Toydemir P, Procter M, Cahalan SM, Kim HJ, Bandell M, Longo N, Day RW, et al. Impaired PIEZO1 function in patients with a novel autosomal recessive congenital lymphatic dysplasia. *Nature communications*. 2015; 6:8329.
- Lynch FM, Izzard AS, Austin C, Prendergast B, Keenan D, Malik RA, Heagerty AM. Effects of diabetes and hypertension on structure and distensibility of human small coronary arteries. *Journal of hypertension*. 2012; 30:384–389. [PubMed: 22124179]

- Mederos y Schnitzler M, Storch U, Meibers S, Nurwakagari P, Breit A, Essin K, Gollasch M, Gudermann T. Gq-coupled receptors as mechanosensors mediating myogenic vasoconstriction. *The EMBO journal*. 2008; 27:3092–3103. [PubMed: 18987636]
- Melchior B, Frangos JA. Gα₁₂/11-mediated intracellular calcium responses to retrograde flow in endothelial cells. *American journal of physiology Cell physiology*. 2012; 303:C467–473. [PubMed: 22700794]
- Mendoza SA, Fang J, Gutterman DD, Wilcox DA, Bubolz AH, Li R, Suzuki M, Zhang DX. TRPV4-mediated endothelial Ca²⁺ influx and vasodilation in response to shear stress. *American journal of physiology Heart and circulatory physiology*. 2010; 298:H466–476. [PubMed: 19966050]
- Navone SE, Marfia G, Invernici G, Cristini S, Nava S, Balbi S, Sangiorgi S, Ciusani E, Bosutti A, Alessandri G, et al. Isolation and expansion of human and mouse brain microvascular endothelial cells. *Nature protocols*. 2013; 8:1680–1693. [PubMed: 23928501]
- Niebauer J, Cooke JP. Cardiovascular effects of exercise: role of endothelial shear stress. *Journal of the American College of Cardiology*. 1996; 28:1652–1660. [PubMed: 8962548]
- Nonomura K, Woo SH, Chang RB, Gillich A, Qiu Z, Francisco AG, Ranade SS, Liberles SD, Patapoutian A. Piezo2 senses airway stretch and mediates lung inflation-induced apnoea. *Nature*. 2017; 541:176–181. [PubMed: 28002412]
- Parry DA, Smith CE, El-Sayed W, Poulter JA, Shore RC, Logan CV, Mogi C, Sato K, Okajima F, Harada A, et al. Mutations in the pH-Sensing G-protein-Coupled Receptor GPR68 Cause Amelogenesis Imperfecta. *American journal of human genetics*. 2016; 99:984–990. [PubMed: 27693231]
- Pathan AR, Rusch NJ. Two-pore domain K(+) channels: evidence for TWIK-2 in blood pressure regulation. *Hypertension*. 2011; 58:539–541. [PubMed: 21876073]
- Ramkhalawon B, Rivas D, Lehoux S. Shear stress activates extracellular signal-regulated kinase 1/2 via the angiotensin II type 1 receptor. *FASEB journal: official publication of the Federation of American Societies for Experimental Biology*. 2013; 27:3008–3016. [PubMed: 23585396]
- Ranade SS, Qiu Z, Woo SH, Hur SS, Murthy SE, Cahalan SM, Xu J, Mathur J, Bandell M, Coste B, et al. Piezo1, a mechanically activated ion channel, is required for vascular development in mice. *Proceedings of the National Academy of Sciences of the United States of America*. 2014; 111:10347–10352. [PubMed: 24958852]
- Retailleau K, Duprat F, Arhatte M, Ranade SS, Peyronnet R, Martins JR, Jodar M, Moro C, Offermanns S, Feng Y, et al. Piezo1 in Smooth Muscle Cells Is Involved in Hypertension-Dependent Arterial Remodeling. *Cell reports*. 2015; 13:1161–1171. [PubMed: 26526998]
- Rode B, Shi J, Endesh N, Drinkhill MJ, Webster PJ, Lotteau SJ, Bailey MA, Yuldasheva NY, Ludlow MJ, Cubbon RM, et al. Piezo1 channels sense whole body physical activity to reset cardiovascular homeostasis and enhance performance. *Nature communications*. 2017; 8:350.
- Schwaderer AL, Schwartz GJ. Back to basics: acidosis and alkalosis. *Pediatrics in review/American Academy of Pediatrics*. 2004; 25:350–357.
- Silvestre JS, Smadja DM, Levy BI. Postischemic revascularization: from cellular and molecular mechanisms to clinical applications. *Physiological reviews*. 2013; 93:1743–1802. [PubMed: 24137021]
- Storch U, Mederos y Schnitzler M, Gudermann T. G protein-mediated stretch reception. *American journal of physiology Heart and circulatory physiology*. 2012; 302:H1241–1249. [PubMed: 22227128]
- Sukharev SI, Blount P, Martinac B, Blattner FR, Kung C. A Large-Conductance Mechanosensitive Channel in *E. coli* Encoded by MscL Alone. *Nature*. 1994; 368:265–268. [PubMed: 7511799]
- Tuttle JL, Sanders BM, Burkhardt HM, Fath SW, Kerr KA, Watson WC, Herring BP, Dalsing MC, Unthank JL. Impaired collateral artery development in spontaneously hypertensive rats. *Microcirculation*. 2002; 9:343–351. [PubMed: 12375172]
- Walker RG, Willingham AT, Zuker CS. A *Drosophila* mechanosensory transduction channel. *Science*. 2000; 287:2229–2234. [PubMed: 10744543]
- Wang N, Naruse K, Stamenovic D, Fredberg JJ, Mijailovich SM, Tolic-Norrelykke IM, Polte T, Mannix R, Ingber DE. Mechanical behavior in living cells consistent with the tensegrity model.

- Proceedings of the National Academy of Sciences of the United States of America. 2001; 98:7765–7770. [PubMed: 11438729]
- Wang S, Chennupati R, Kaur H, Iring A, Wettschureck N, Offermanns S. Endothelial cation channel PIEZO1 controls blood pressure by mediating flow-induced ATP release. *The Journal of clinical investigation*. 2016; 126:4527–4536. [PubMed: 27797339]
- Woo SH, Ranade S, Weyer AD, Dubin AE, Baba Y, Qiu Z, Petrus M, Miyamoto T, Reddy K, Lumpkin EA, et al. Piezo2 is required for Merkel-cell mechanotransduction. *Nature*. 2014; 509:622–626. [PubMed: 24717433]
- Yan L, Singh LS, Zhang L, Xu Y. Role of OGR1 in myeloid-derived cells in prostate cancer. *Oncogene*. 2014; 33:157–164. [PubMed: 23222714]
- Yan Z, Zhang W, He Y, Gorczyca D, Xiang Y, Cheng LE, Meltzer S, Jan LY, Jan YN. Drosophila NOMPC is a mechanotransduction channel subunit for gentle-touch sensation. *Nature*. 2013; 493:221–225. [PubMed: 23222543]
- Zhang YL, Frangos JA, Chachisvilis M. Mechanical stimulus alters conformation of type 1 parathyroid hormone receptor in bone cells. *American journal of physiology Cell physiology*. 2009; 296:C1391–1399. [PubMed: 19369447]

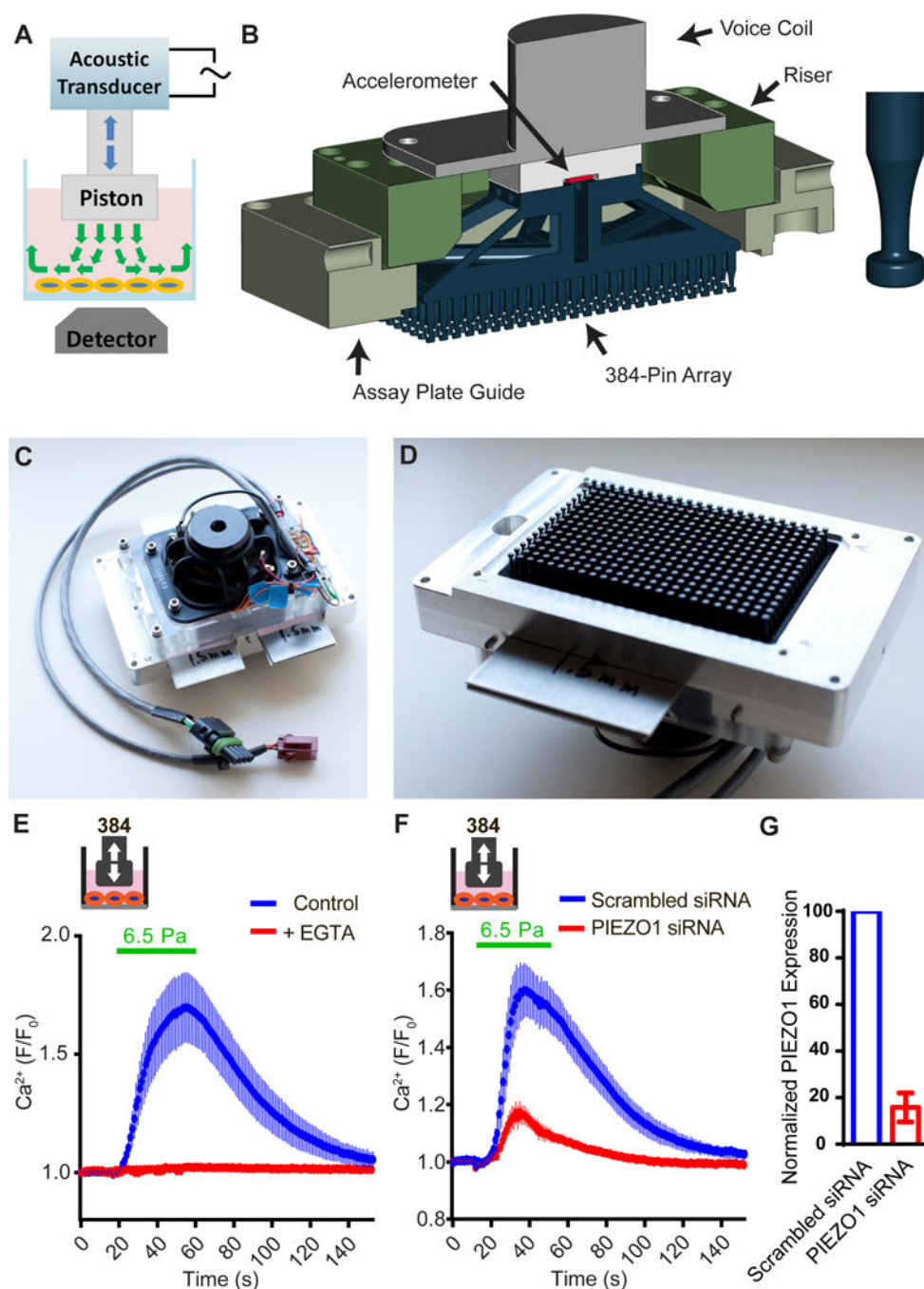
Highlights

Description of a high throughput assay for cellular mechanosensation

an RNAi screen identifies GPR68 is as a mechanosensor

GPR68 is necessary and sufficient for responses to shear stress

GPR68 is required for flow-induced dilation and remodeling in mice



for each condition. (E) Intracellular calcium levels of HeLa cells under the same disturbed flow stimulation after the treatment of scrambled siRNA or hPIEZO1 siRNA. Data is average of 48 wells from 3 trials for each condition. (F) Relative mRNA level of PIEZO1 in HUVECs transfected with PIEZO1 siRNA compared with cells treated with scrambled siRNA (n=3).

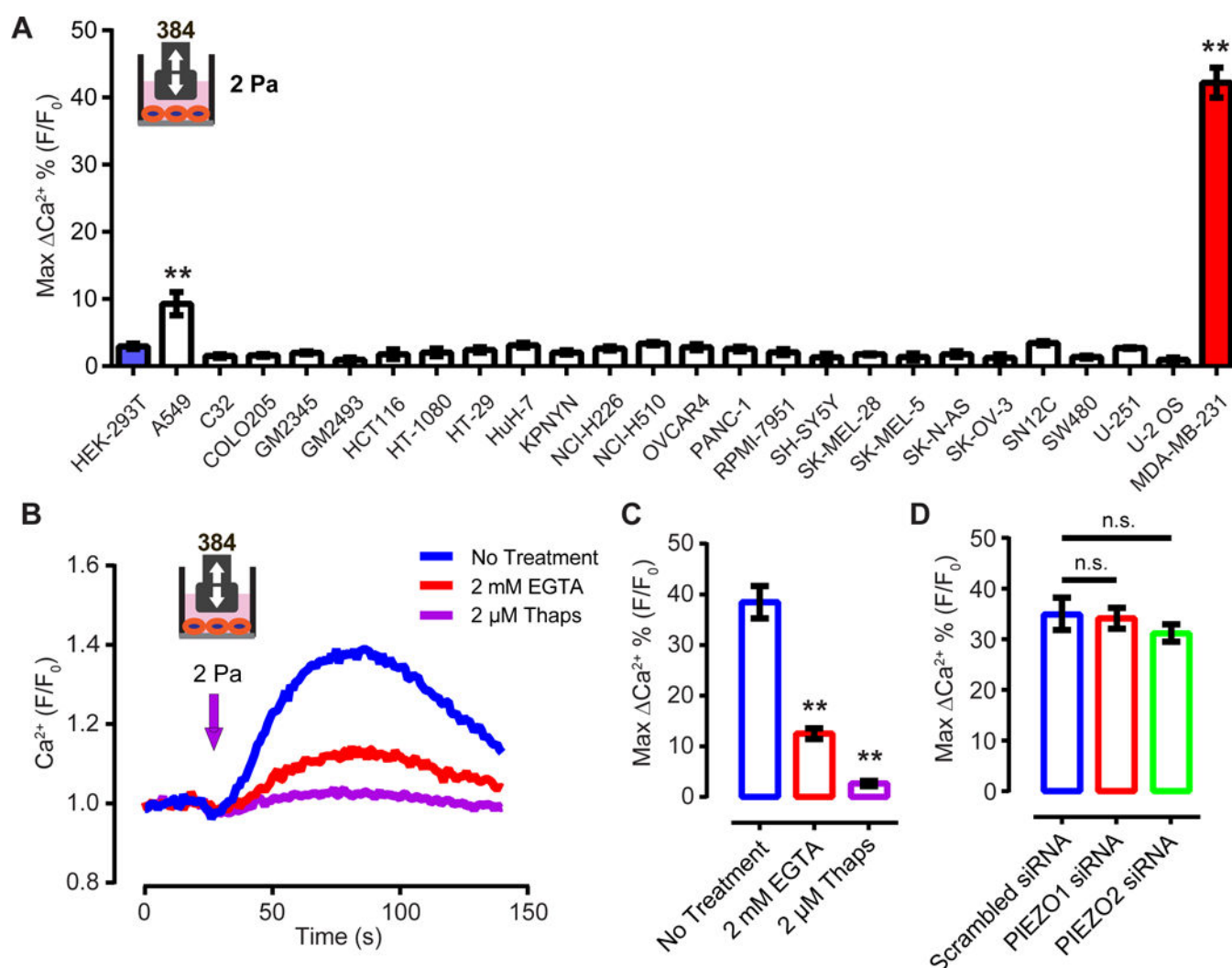


Figure 2. MDA-MB-231 cells show PIEZO1- and PIEZO2-independent shear stress-induced calcium transients

(A) Responses of various human cancer cell lines to shear stress at 2 Pa, 60 Hz, with 0.2 s on, 2s off for 40 s. ** $p < 0.01$ (B) The response of MDA-MB-231 cells to shear stress at 2 Pa, measured by FLIPR. The shear stress was applied for 4 s at 60 Hz. EGTA was added to the cells 2 min prior to the onset of shear stress. Thapsigargin was incubated with cells for 15 min before the shear stress stimulation. (C) Quantification of the MDA-MB-231 cells' response to shear stress in the presence of the EGTA and thapsigargin. ** $p < 0.01$. (D) Quantification of the MDA-MB-231 cells' response to shear stress 72 h after transfection of PIEZO1 and PIEZO2 siRNA. n.s., not significant.

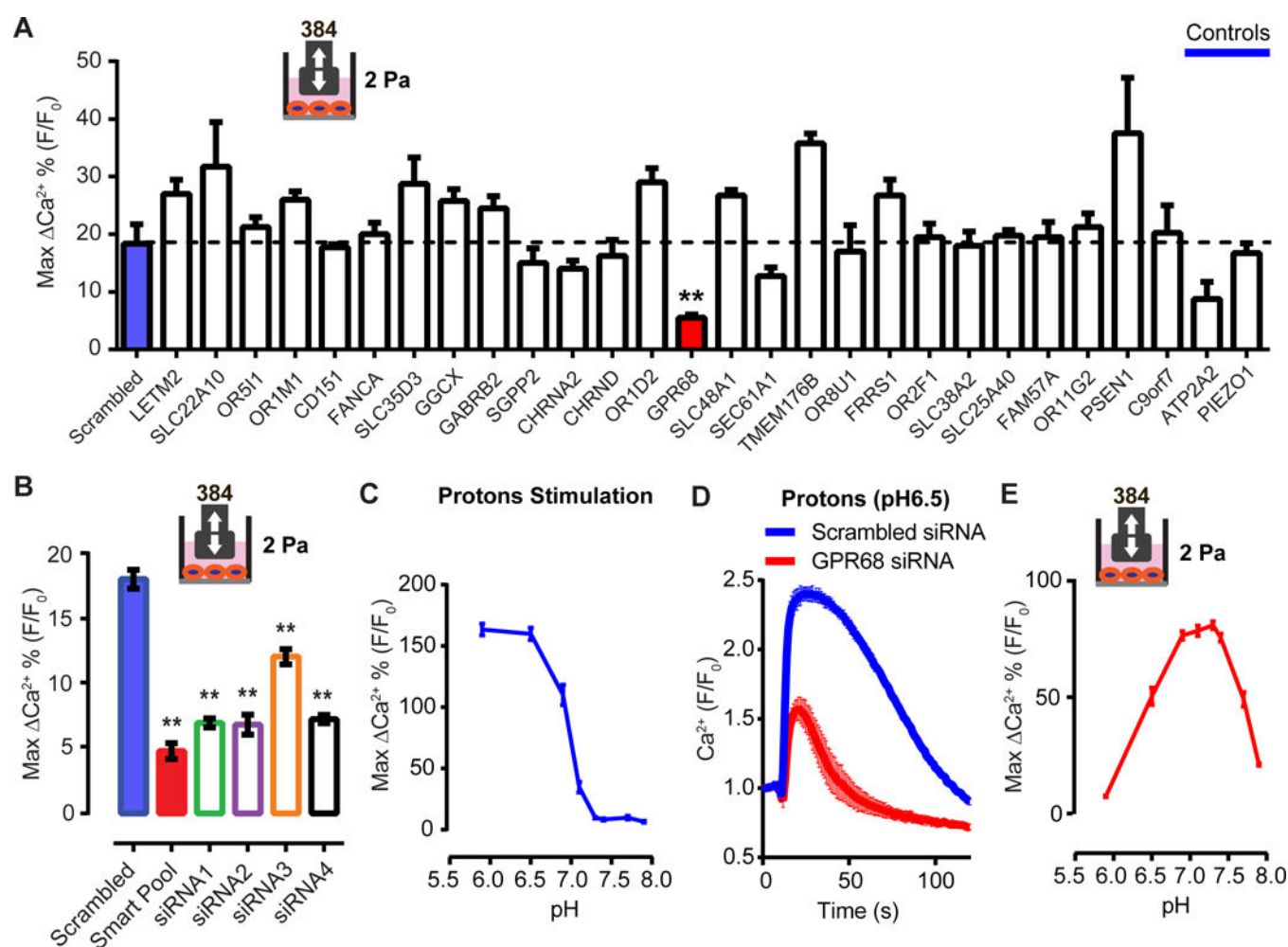


Figure 3. GPR68 is necessary for shear stress-induced calcium transients in MDA-MB-231 cells
 (A) The response of MDA-MB-231 cells after treatment of siRNAs against the indicated candidates. ** $p < 0.01$ (B) Quantification of the MDA-MB-231 cells' response to shear stress after treatment with smartpool siRNA oligos and the individual siRNA oligos against GPR68. ** $p < 0.01$. (C) Response of MDA-MB-231 cells to proton stimulation at various final pH. The cells were incubated with HBSS at pH7.4 before the addition of the HBSS with various acidity. $n = 3$. (D) The response of MDA-MB-231 cells to proton stimulation (final pH 6.5) after knocking down GPR68 by siRNA smartpool. (E) The response of MDA-MB-231 cells to shear stress stimulation in buffers with various pH. The cells were incubated with assay buffer at pH7.4. The pH was then changed by adding buffer with various acidity 3 min prior to the onset of shear stress stimulation.

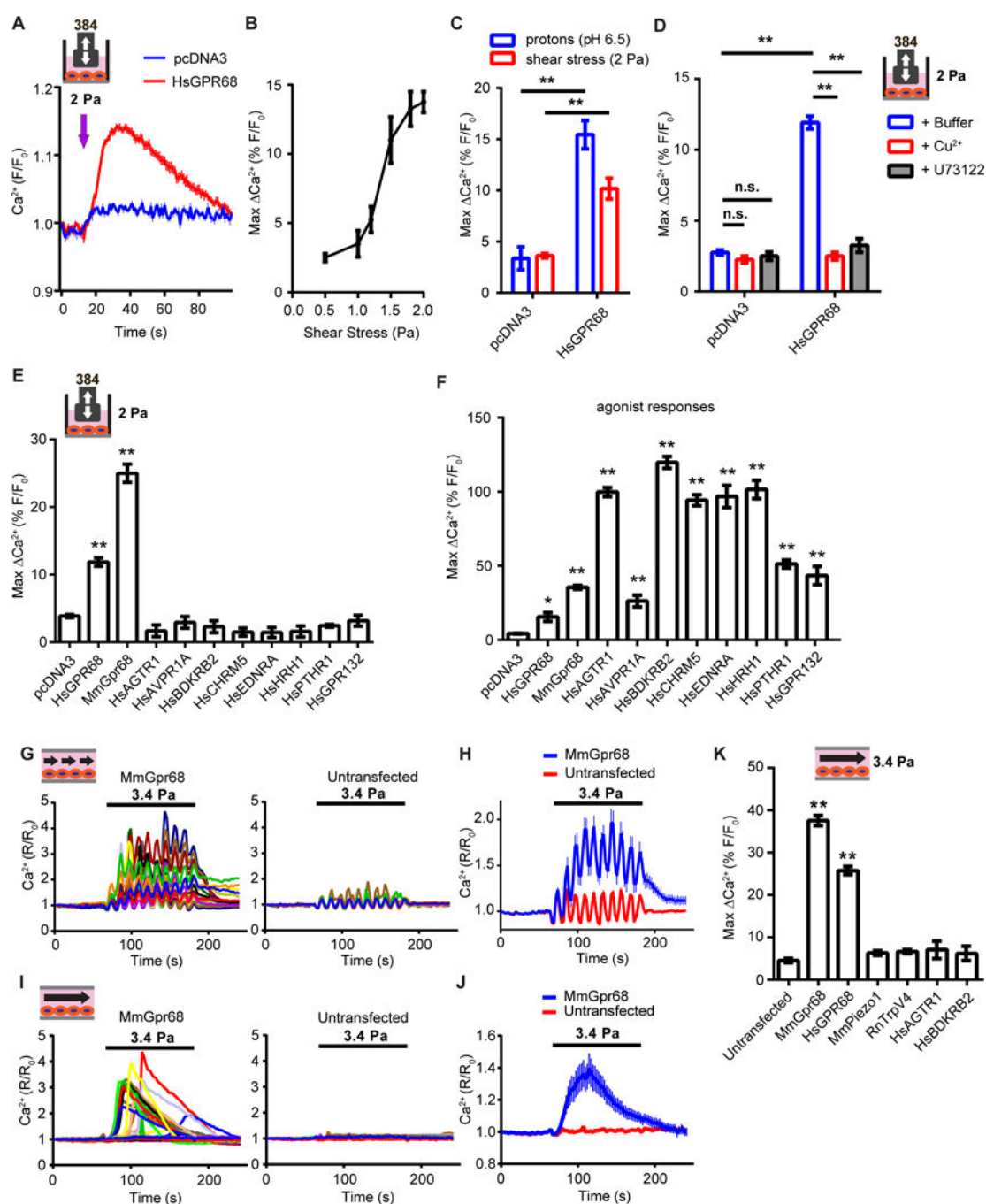


Figure 4. GPR68 is sensitive to shear stress imposed by both disturbed and laminar flow in HEK-293T cells

(A) Disturbed flow-induced calcium transients in HEK-293T cells transfected with human GPR68 or vector control 48 h before the assay. Flow was applied at 60 Hz for 4s (arrow indicates the onset of the flow). (B) Quantification of the amplitude of the calcium transients evoked by disturbed shear stress of increasing intensities. n=3 wells per intensity tested. (C) Response of HEK-293T cells to pH 6.5 stimulation and 2 Pa disturbed shear stress. ** p<0.01. (D) Response of HEK-293T cells to 2 Pa disturbed flow in the presence of 20 μM Cu^{2+} or 10 μM U73122. Cu^{2+} or U73122 was added to the assay buffer 2 min prior to the

start of the flow. n.s., not significant. ** $p < 0.01$. (E) The shear stress induced responses of HEK-293T cells transiently-transfected with various human and mouse GPCRs. ** $p < 0.01$. (F) The agonist response of HEK-293T cells transiently-transfected with various human and mouse GPCRs. ** $p < 0.01$. The chemical activators used were: pH 6.5 for human and murine GPR68, 0.5 μ M Angiotensin II for AGTR1, 0.5 μ M [Arg⁸]-Vasopressin for AVPR1A, 0.5 μ M Bradykinin for BDKRB2, 0.5 μ M Acetylcholine Chloride for CHRM5, 0.5 μ M Endothelin I for EDNRA, 0.5 μ M Histamine Dihydrochloride for HRH1, 20 μ M Parathyroid Hormone (1-34) for PTHR1, and 100 mM lactate for GPR132. (G) Representative traces of intracellular calcium levels in HEK-293T cells transfected with mouse Gpr68-IRES-eGFP upon pulsatile laminar flow stimulation. Cells with GFP signal were considered transfected and the GFP negative ones were untransfected. Pulsatile laminar flow was applied at 3.4 Pa, 1 Hz for 120 s. (H) Quantification of the response of HEK cells to pulsatile laminar flow. $n=172$ for MmGpr68 transfected and 165 for untransfected. (I) Representative traces of intracellular calcium levels in HEK-293T cells transfected with mouse Gpr68-IRES-eGFP upon steady laminar flow stimulation. Steady laminar flow was applied at 3.4 Pa for 120 s. (J) Response of HEK cells to steady laminar flow. $n=162$ for MmGpr68 transfected and 183 for untransfected. (K) Responses of HEK-293T cells transfected with various putative mechanosensors to steady laminar flow at 3.4 Pa. ** $p < 0.01$.

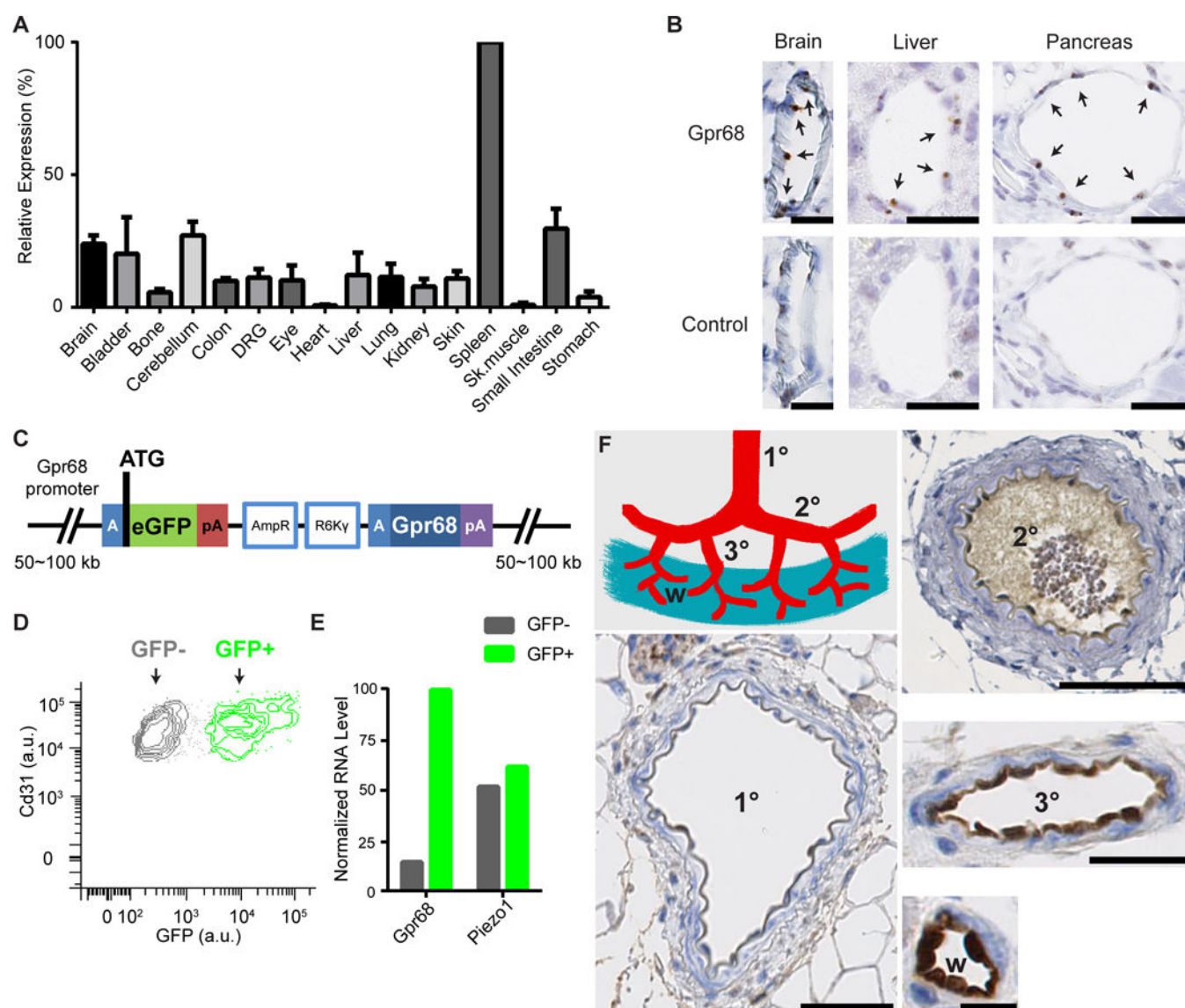


Figure 5. GPR68 expression is detected in endothelial cells of small-diameter vessels
 (A) Murine Gpr68 mRNA expression profile determined by qRT-PCR. Gapdh was used as the reference gene. The expression levels were normalized to spleen. n=2~3. (B) Representative images of colorimetric RNAscope *in situ* hybridization for Gpr68 vascular endothelial cells of small diameter blood vessels in brain, pancreas and liver. Scale bars: 25 μ m. Arrows indicate cells with positive signal. (C) Schematic diagram of the BAC transgenic construct that is integrated in the genome of Gpr68 eGFP reporter mice. The blue A-box is the homologous sequence that guides recombination and insert eGFP after the start codon of Gpr68. Poly-A sequence following the eGFP blocks the transcription of the downstream genes within the construct (including Gpr68). pA: poly-A sequence; AmpR, ampicillin-resistance genes; R6K γ , origin of DNA replication (AmpR and R6K γ are used in the initial selection of BAC constructs). (D) FACS plot of primary endothelial cells isolated from the bladder of Gpr68-eGFP reporter mice. Cells that are CD31+ and CD45- are shown, and grouped in the GFP+ and GFP- populations. (E) Normalized RNA levels

(RPKM) of Gpr68 and Piezo1 from the RNAseq data of GFP⁺ and GFP[−] endothelial cells. Bladder cells from 3 batches of isolation and sorting (10 mice in total) were pooled and subjected to RNAseq. (F) Representative images of GFP antibody staining in arteries of 1st order (1°), 2nd order (2°), 3rd order (3°) superior mesenteric vessels, and the vessels in the wall of small intestine (w). Scale bars: 50 μm for 1° and 2° vessels, 25 μm for 3° vessels, and 10 μm for vessels in the small intestine wall. 8 groups of vessels from 4 mice were examined.

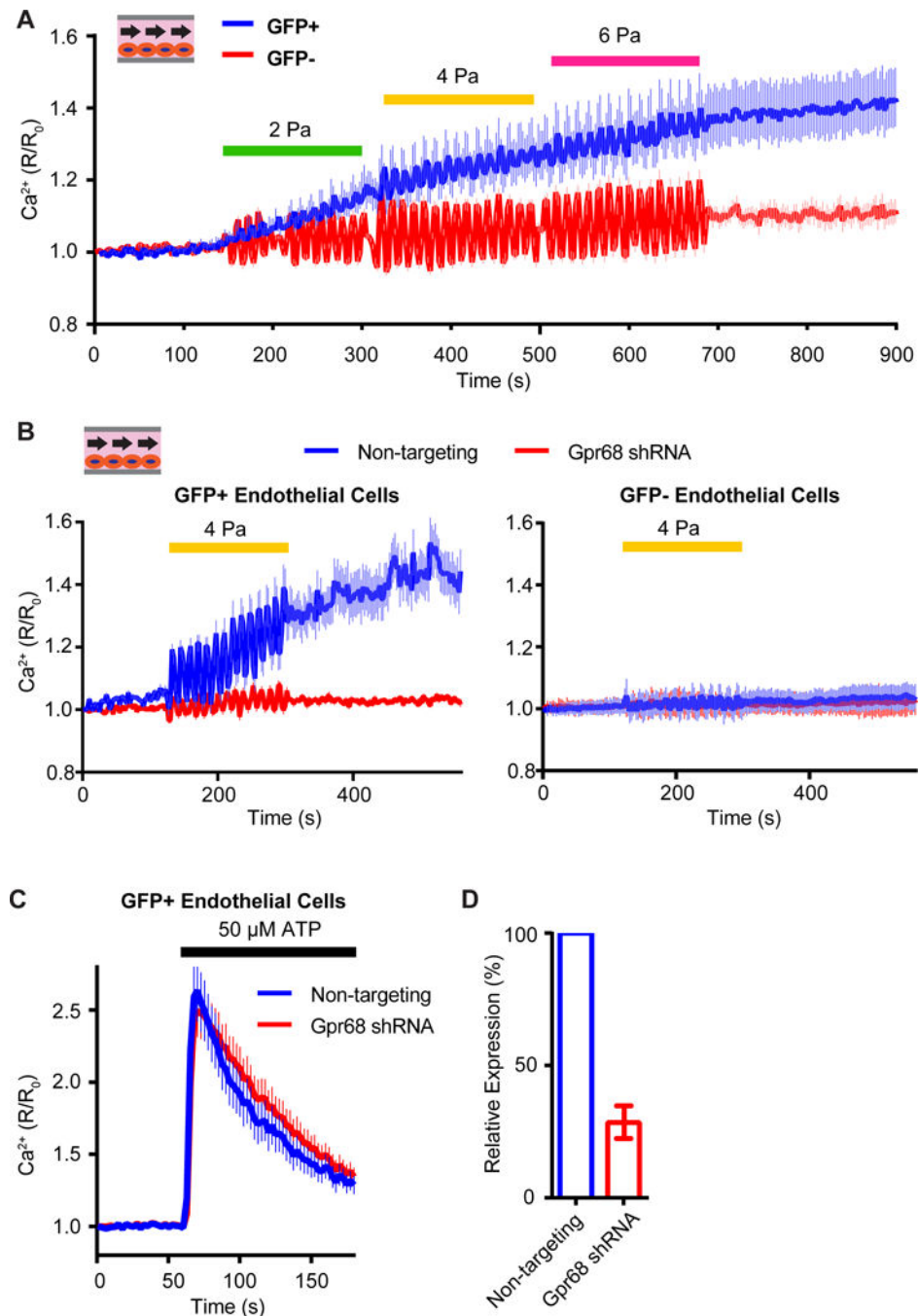


Figure 6. Gpr68 is necessary for laminar flow-induced calcium transients in murine primary microvascular endothelial cells

(A) Responses of mouse primary microvascular endothelial cells (MVECs) to shear stress imposed by pulsatile laminar flow with increasing amplitudes. The MVECs were isolated from cerebrum of the Gpr68 eGFP reporter mice. Pulsatile laminar flow of different amplitudes are applied at 1 Hz for 180s. n=148 (GFP+) and 155 (GFP-). Data is pooled from 3 trials. (B) Responses of GFP+ and GFP- MVECs to pulsatile laminar shear stress at 4 Pa. The MVECs were infected with lentivirus containing non-targeting shRNA or Gpr68 shRNA constructs. The pulsatile flow is applied at 1 Hz for 180 s. n=166 (non-targeting) and

173 (Gpr68 shRNA). 3 trials. (C) The calcium transients in primary MVECs induced by to 50 μ M ATP. n=223 (non-targeting) and 198 (Gpr68 shRNA). 3 trials. (D) Quantification of the knockdown efficiency of lentiviral shRNA against Gpr68. n=3.

Author Manuscript

Author Manuscript

Author Manuscript

Author Manuscript

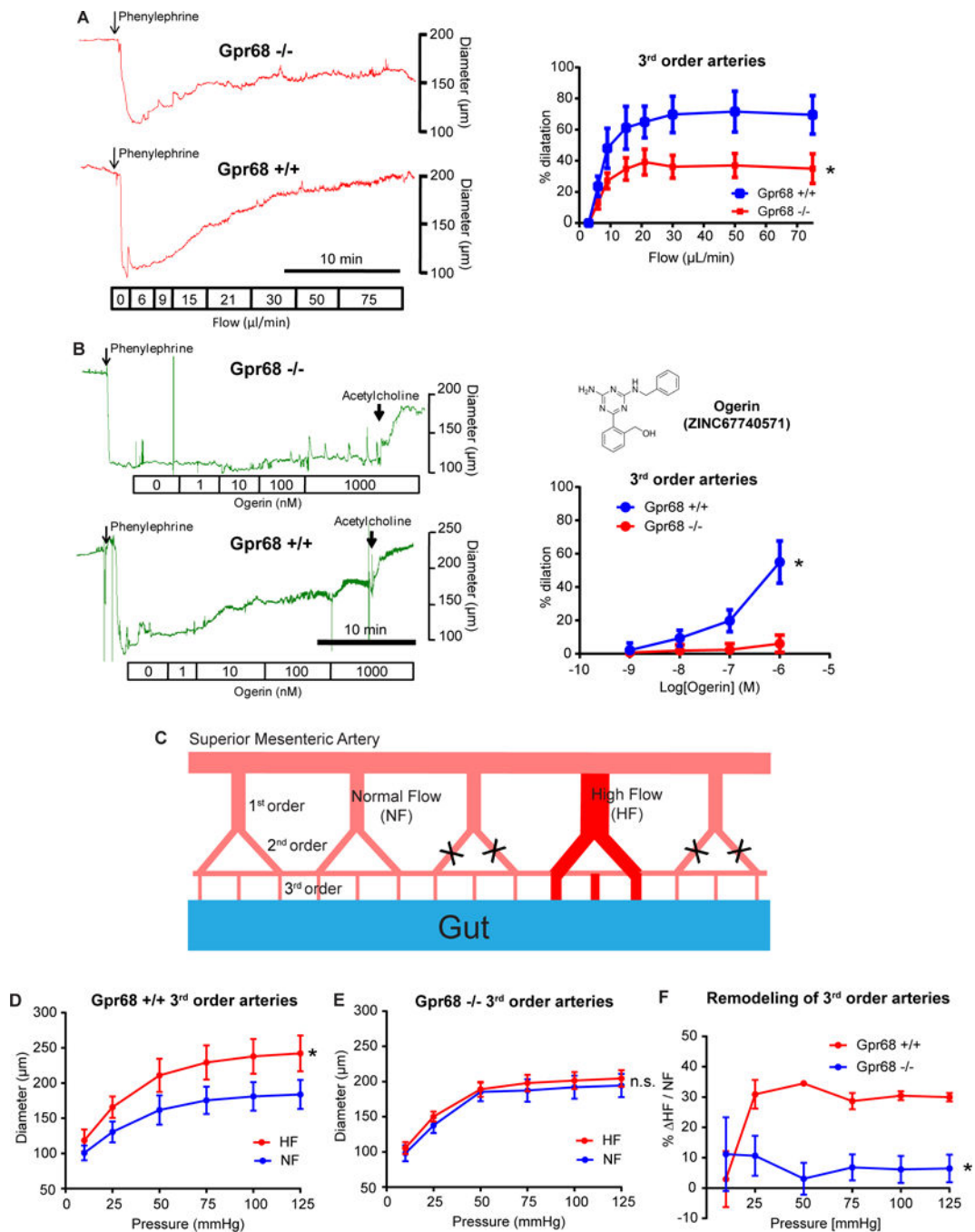


Figure 7. Gpr68 is required for flow-mediated dilation and outward remodeling in third order mesenteric arteries (MAs)

(A) Flow-mediated dilation (FMD) response of third order MAs isolated from Gpr68 $-/-$ mice and WT littermates. Vessels were cannulated and pre-constricted using 1 μM phenylephrine, and subjected to stepwise increases in flow rates. Left, representative recordings of vessel diameter change. Scale bar: 10 minutes. Right, quantification of FMD response in 3rd order MAs. $p=0.044$, two way ANOVA, $n=9$ for Gpr68 KO and $n=7$ for WT. (B) Dilation responses of third order MAs to Ogerin. Vessels were cannulated and pre-constricted using 1 μM phenylephrine, and subjected to Ogerin with increasing

concentration. Left, representative recordings of vessel diameter change. Scale bar: 10 minutes. Right, quantification of Ogerin-induced dilation 3rd order MAs. Vessels from 6 KO and 6 WT mice were tested. $P=0.018$, two way ANOVA. Inset, structure of Ogerin. (C) Schematic representation of the surgery applied to mesenteric arteries to create local high flow (HF) and normal (NF) regions (see EXPERIMENTAL PROCEDURE). (D, E) Flow-mediated remodeling (FMR) of 3rd order mesenteric arteries isolated from WT ($P=0.0045$) and Gpr68 KO mice ($P=0.95$). (F) The extent of outward remodeling as indicated by the percentage of vessel diameter increase ($*P=0.0309$). $*p<0.05$, two way ANOVA for repeated measures, $n=5$ for Gpr68 $-/-$ and $n=7$ for WT.